A computational view of the brain plasticity at rest

Invernizzi, Azzurra

DOI:
10.33612/diss.183130118

Chapter 2

Bayesian Connective Field Modelling using a Markov Chain Monte Carlo approach

Under review.

Invernizzi A
Haak KV
Carvalho JC
Renken RJ
Cornelissen FW.

ABSTRACT

The majority of neurons in the human brain process signals from neurons elsewhere in the brain.

Connective Field (CF) modelling is a biologically-grounded method to describe this essential aspect of the brain's circuitry. It allows characterizing the response of a population of neurons in terms of the activity in another part of the brain. CF modelling translates the concept of the receptive field (RF) into the domain of connectivity by assessing, at the voxel level, the spatial dependency between signals in distinct cortical visual field areas. Thus, the approach enables to characterize the functional cortical circuitry of the human cortex. While already very useful, the present CF modelling approach has some intrinsic limitations due to the fact that it only estimates the model's explained variance and not the probability distribution associated with the estimated parameters. If we could resolve this, CF modelling would lend itself much better for statistical comparisons at the level of single voxels and individuals. This is important when trying to gain a detailed understanding of the neurobiology and pathophysiology of the visual cortex, notably in rare cases. To enable this, we present a Bayesian approach to CF modeling (bCF). Using a Markov Chain Monte Carlo (MCMC) procedure, it estimates the posterior probability distribution underlying the CF parameters. Based on this, bCF quantifies, at the voxel level, the uncertainty associated with each parameter estimate. This information can be used in various ways to increase confidence in the CF model predictions. We applied bCF to BOLD responses recorded in the early human visual cortex using 3T fMRI. We estimated both the CF parameters and their associated uncertainties and show they are only weakly correlated. Moreover, we show how bCF facilitates the use of effect size (beta) as a data-driven parameter that can be used to select the most reliable voxels for further analysis. Finally, to further illustrate the functionality gained by bCF, we apply it to perform a voxel-level model comparison which suggests that, unlike stimulus driven pRFs, neural referred CFs may not possess a spatial center-surround organisation. We conclude that our bCF framework provides a comprehensive tool to study human functional cortical circuitry in health and disease.

Highlights

- We present a Bayesian variant of the Connective Field (bCF) modeling framework.
- A MCMC procedure quantifies the uncertainty associated with each CF parameter which can be used in various ways to increase confidence in the model predictions.
- Effect size (beta) can be used as a data-driven threshold to retain relevant voxels.
- The CFs of the human early visual system are best described by a single, circular symmetric, Gaussian.

2.1 INTRODUCTION

Over the past decades, the use of functional magnetic resonance imaging (fMRI) combined with a rapid development of biologically-grounded computational models has enabled a deep understanding of the function of cortical areas of the human visual system (Wandell and Wade 2003; Park, Shin, and Lee 2002; Meindertsma et al. 2017; Dumoulin and Wandell 2008; Zeidman et al. 2018; Adaszewski et al. 2018; Benson and Winawer 2018; Wandell and Winawer 2015). However, what is still less well understood is how the cortical circuitry that connects these different cortical areas shapes their interactions and, ultimately, supports their functions. Indeed, the majority of the neurons in the human brain process and integrate signals from neurons elsewhere in the brain (Robinson 1989). The resulting spatial and temporal interactions and integration result in cortical feedback and feedforward mechanisms that enable key brain functions such as human perception and attention.

One possible approach to describe the cortical circuitry underlying such cortico-cortical interactions is connective field (CF) modelling (Haak V. et al. 2013). CF modeling allows characterizing the cortical response properties of a population of neurons in terms of the activity in another region of the visual cortex. In essence, it translates the concept of the stimulus-referred receptive field (RF) into the domain of connectivity by assessing the spatial dependency between signals in distinct cortical visual field areas (Haak V. et al. 2013). This neural-referred RF is also known as the cortico-cortical population RF (cc-pRF). The CF approach can be used to assess the spatial integration properties of the visual system from either task-evoked or resting-state neural responses (Gravel et al. 2014; Bock et al. 2015). So far, it has been mainly used to study connective plasticity in various ophthalmic and neurological diseases (Haak, Morland, and Cornelissen 2013; Halbertsma, Haak, and Cornelissen 2019; Haak V. et al. 2016; Ahmadi et al. 2019; Carvalho, Renken, and Cornelissen 2019; De Best et al. 2019).

Unfortunately, the standard CF (sCF) approach has some intrinsic properties which limit its use in a variety of potential applications. These limitations are due to the fact that the optimal model fit is obtained by minimizing the difference between the prediction and measured signal on the basis of minimizing the residual sum of squares (RSS). Consequently, model comparison is only possible based on the percentage of explained variance of the model and there is no information to quantify the variability and reliability of the various estimated CF parameters. If we could retrieve the latter type of information, CF modelling would lend itself much better for statistical comparisons at the level of single individuals, which can be important in the context of patient studies, e.g. with a neurodegenerative disorder, such as glaucoma. There, it would be

critical to also understand the reliability of the estimates in each patient. This would be even essential when assessing rare cases, where group averages are not available. Moreover, it would become possible to evaluate the probability of CF models at the level of single voxels. This may help to unravel the detailed neurobiology of the visual cortex by testing alternative models to explain task or resting-state related responses (e.g. comparing different receptive field shapes while taking model complexity into account). The present limitations of the CF modeling approach may be overcome by determining the full underlying probability distributions for the various CF parameters. From these, we can quantify, at the voxel level, the uncertainty associated with each parameter estimate. Theoretically, uncertainty is a useful evaluation parameter by itself. First of all, it can establish confidence in the CF model predictions. Secondly, it may be valuable for investigating and meaningfully explaining differences within parameter distributions as a result of different conditions, tasks, interventions or pathology. Finally, it may be used to identify model biases that, for example, result from over- or under-fitting or a co-dependence of parameters. Removing such dependencies may help to further improve the CF model predictions.

To enable this new functionality, we present a Bayesian inference framework for CF modelling, which we will refer to with bCF. Using a Markov Chain Monte Carlo (MCMC) procedure (Robert and Casella 2011), bCF provides the underlying posterior probability distribution of the CF parameters (position and size in case of the most basic model). From this distribution, we can derive the uncertainty associated with each of these parameters. In addition, we also retain the effect size of the CF model, which we will refer to as beta (adhering to the nomenclature used by (Zeidman et al. 2018)). We show how beta can be used as a data-driven threshold. To further illustrate the functionality gained by bCF we show that, at the voxel level, single Gaussian (SG) models are favoured over Difference-of-Gaussian (DoG) models. This suggests that, unlike stimulus-driven pRFs, the cortico-cortical RFs of the early visual system do not possess a center-surround organisation.

2.2 METHODS

2.2.1 Participants

Twelve healthy female participants (mean age 22 years, s.d. = 1.8 years) with normal or corrected-to-normal vision and without a history of neurological disease were included. Previously, these data have been used as a normative dataset in work that did not use our present framework (Halbertsma, Haak, and Cornelissen 2019). Anonymised and preprocessed time series for each visual area can be downloaded at this link: http://www.visualneuroscience.nl/cf.

The ethics board of the University Medical Center Groningen (UMCG) approved the study protocol. All participants provided written informed consent. The study followed the tenets of the Declaration of Helsinki.

2.2.2 Stimuli presentation and description

The visual stimuli were displayed on a MR compatible screen located at the head-end of the MRI scanner with a viewing distance of 118 cm. The participant viewed the complete screen through a mirror placed at 11 cm from the eyes and supported by the 32-channel SENSE head coil. Screen size was 36 x 23 degrees of visual angle and the distance from the participant's eyes to the screen was approximately 75 cm. Stimuli were generated and displayed using the Psychtoolbox (http://psychtoolbox.org/) and VISTADISP toolbox (VISTA Lab, Stanford University), which are both MatLab based (Brainard 1997; Pelli 1997). The stimulus consisted of drifting bar apertures (of 10.2 deg radius) with a high contrast checkerboard texture on a grey (mean luminance) background. A sequence of eight different bar apertures with four different bar orientations (horizontal, vertical and diagonal orientations), two opposite motion directions and four periods of mean-luminance presentations comprised the stimulus presentation that lasted 192 second. The bar contrast, width and spatial frequency were respectively 10%, 2.5 degrees and 0.5 cycles per degree. After each pass and a half, 12 seconds of a blank stimulus at mean luminance was presented full screen. To maintain stable fixation, participants were instructed to focus on a small colored dot present in the center of the screen and press a button as soon as the dot changed color. The complete visual field mapping paradigm was presented to the participant six times, with a new scan started for each repetition.

2.2.3 Data acquisition

MRI and fMRI data were obtained using a 3T Philips Intera MRI scanner (Philips, the Netherlands), with a 32-channel head coil. For each participant, a high-resolution T1-weighted three-dimensional structural scan was acquired (TR = 9.00ms, TE = 3.5ms, flip-angle = 8, acquisition matrix = 251*251*170mm, field of view = 256x170x232, voxel size = 1x1x1mm). Six visual field mapping (VFM) functional T2*-weighted, 2D echo planar images were obtained (voxel resolution of 2.5x2.5x2.5, field of view = 190x190x50 mm, TR = 1500ms, TE = 30ms). Each VFM scan lasted for 192s with a total of 136 volumes. A short T1-weighted anatomical scan with the same field of view chosen for the functional scans were acquired and used for obtaining a better co-registration between functional and anatomical volume.

2.2.4 Standard fMRI data analysis

Preprocessing and standard (pRF and CF) analyses of fMRI data were done using ITKGray (http://www.itk.org) and the mrVista toolbox for MatLab (VISTASOFT, https://

github.com/vistalab/vistasoft; http://www.white.stanford.edu). The Bayesian CF approach and Bayesian CF model comparison were developed and performed using MatLab 2016b (The Mathworks Inc., Natick, Massachusetts).

2.2.4.1 Preprocessing

For each participant, the structural scan was reoriented using the anterior commissure-posterior commissure line (AC-PC line) as reference. Next, grey and white matter were automatically segmented using Freesurfer, and manually adjusted using ITKGray to minimize possible segmentation errors.

All functional data were pre-processed and analysed using the mrVista toolbox. First, motion correction within and between scans was applied. Then, we performed an alignment of functional data into anatomical space and lastly, an interpolation of functional data onto the segmented anatomical grey and white matter obtained using the ITKGray/Freesurfer.

2.2.4.2 Population Receptive Field (pRF) mapping

Retinotopy scans were analyzed using a model-based analysis, known as the population receptive field (pRF) method (Dumoulin and Wandell 2008), which allows localizing the visual field maps of interest. Based on the best fitting prediction obtained using a 2D Gaussian model, the hemodynamic response (HRF), and the stimulus aperture, we estimate the visual field mapping parameters (eccentricity, polar angle and pRF size). The best model fit was projected onto a smoothed 3D mesh of the cortex, on which the visual areas were functionally identified using standard techniques (Wandell and Winawer 2015; Sereno, McDonald, and Allman 1994; Engel, Glover, and Wandell 1997). Based on the phase reversals in the pRF maps, visual cortical areas (V1, V2, V3, hV4, LO1 and LO2) were located and manually delineated for each participant individually and according to standard criteria (Dumoulin and Wandell 2008). These areas were then used to define the target and the source regions for the CF analysis.

2.2.4.3 Standard connective field modelling

In short, in the standard CF approach (Haak V. et al. 2013), the optimal CF model parameters are estimated in order to explain an observed signal of a single voxel in a target region (e.g. V2 or V3) based on the signals in a source region (e.g. V1). To do so, a 2D Gaussian CF model (with parameters position and size) is convolved with the BOLD time series of the voxels in the source region in order to calculate a predicted time series. The optimal fit of the model is determined by minimizing the difference between the predicted and observed time series of the target voxel (by minimizing the residual sum of squares (RSS)). The center of the CF is restricted to a voxel location in the source region. For each voxel in the target region, the parameter values that result in an optimal model fit are estimated and retained.

2.2.4.4 Visualizing Connective Field model parameters

For visualization purposes and qualitative analyses, the CF model parameters obtained for each voxel can be projected onto a smoothed 3D mesh of the cortical surface. The CF position on the cortex can be converted from cortical units (in mm) into visual field map units (eccentricity, polar angle; in degrees of visual angle). This is done via a weighted integration of the visual field map properties, estimated via pRF mapping (section 2.4.2), of the voxels encompassed by the CF in the source region.

2.2.5 Bayesian connective field modelling

As in the standard approach, Bayesian CF modelling tries to explain the observed signal of a voxel in a target region based on the signals in a source region. However, rather than estimating only the optimal parameters, the Bayesian approach estimates the full underlying posterior probability distribution associated with each CF parameter. This requires an extensive and iterative sampling of the parameter space of the model which is done using a Markov Chain Monte Carlo (MCMC) procedure. The parameter space of the model is spanned by the following parameters: the CF center (location on a mesh grid that contains the location of all the voxels of the source area), the CF size, and the CF effect size (which scales the amplitude of the predicted to that of the observed signal). At each MCMC iteration, new values for the parameters are proposed and compared to that of the current one, based on the MCMC convergence criteria. Depending on the outcome of this comparison, the proposed model parameters are accepted or not. The rejected values for the model parameters are neither stored nor used for estimating the CF parameters. For each target voxel, a total of 17500 iterations are run, of which the first 10% are discarded to allow for burn-in (Liu, Nordman, and Meeker 2016; Chib 2011). The posterior distributions are estimated based on the samples of the remaining iterations. Throughout, we will use the abbreviation bCF to indicate the Bayesian CF approach. The code for the bCF framework can be obtained via http://www.visualneuroscience.nl/cf. The next sections describe the model (2.5.1), the two parameter estimation options for the MCMC procedure (2.5.2), the CF model parameters, the latent variables, and their priors (2.5.3). We will follow the nomenclature of (Zeidman et al. 2018). An overview of the bCF approach is presented in Figure 1. The latent variables (L) are presented in table 1.

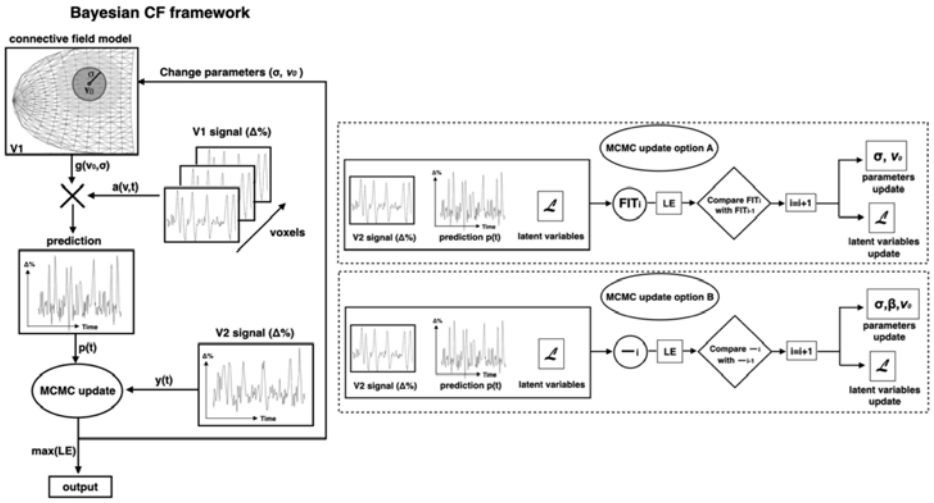

Figure 1 - Overview of the Bayesian CF framework. In this example, we use the bCF approach to estimate the V1➤V2 connective field (i.e. we estimate the source region in V1 of a V2 target voxel). Following the CF definition of Haak et al. (2013), the predicted time series $p(t)$ is obtained by the overlap between a 2D symmetric Gaussian $g(v)$ and the neuronal population inputs $a(v,t)$, which are the fMRI times series of all the voxels in the source region (in this case V1). In the MCMC procedure, the predicted time series $p(t)$, the observed time serie of the (in this case V2) target voxel $y(t)$ and the latent variables ($\mathcal{L}$) are used to define and estimate the CF parameters. Based on the maximum likelihood associated with the error (MLE) calculated between $p(t)$ and $y(t)$, the latent variables (L) are updated for use in the next iteration. Two different MCMC update options are provided: in option A, the likelihood estimation is obtained after scaling *p(t)* using an OLS method thereby estimating the effect size (indicated by FIT in the figure). In option B, the amplitude/scaling parameter (β) is jointly estimated with the other CF parameters and retained for further analyses - the fitting procedure used in this option is indicated by ($-_i$). Figure adapted from Haak et al. (2013).

Table 1 - Latent variables definitions.

	Latent variables ($\mathcal{L}$)	
Bayesian CF model	SG	DoG
Option A	l_s l_σ	l_s l_σ $l_{\sigma 2}$
Option B	l_s l_σ l_β	l_s l_σ l_β $l_{\sigma 2}$ $l_{\beta 2}$

Rows list the latent variables used in the two bCF estimation options for both the single Gaussian (SG) and Difference of Gaussian (DoG) models (see section 2.5.1 and 2.5.4). Latent variables are used for the following reason: in order to obtain a likelihood on a model, it is beneficial to have (latent) parameters, e.g. $l_{\sigma'}$ follow a gaussian distribution. At the same time, the CF parameters are constrained. For example σ is bound to be between 0 and 10 mm. The transformation from latent to non-latent variable allows us to go from the latent variable defined on the interval $-\infty$ and $+\infty$ distribution to the CF variable with compact support.

2.2.5.1 Model definition

The CF model generates a predicted time series $p(t)$ to explain an observed time series $y(t)$ of a target voxel (Eq. 1). To generate $p(t)$, a CF $g(v)$ is convolved with the observed

time series of the voxels (v) in a source $a(v,t)$ (with a representing the neuronal population input based on the BOLD signal change (Δ%)(Eq. 2). The CF $g(v)$ is, in its most elementary form, a 2D circular symmetric Gaussian with a width sigma (σ) (Eq. 3).

$$y(t) = p(t)\beta + \epsilon \quad (1)$$
$$p(t) = \sum_v [\, a(v,t) * g(v)] \quad (2)$$
$$g(v) = exp - [D(v, v_0)^2 / 2\sigma^2] \quad (3)$$

In Eq. 1, β defines the effect size and ϵ is the error term. In Eq. 3, the Gaussian CF $g(v)$ is defined in terms of distance along the cortical surface. Therefore, for all the voxels (v) in the source, the distance matrix $D(v, v_o)$ contains their shortest distances to the CF center (v_o) along a triangular mesh representation of this cortical surface manifold. These distances are computed using Dijkstra's algorithm (Dijkstra 1959). Note that $g(v)$ is scaled to ensure that the total area under the gaussian surface, as calculated across the entire source region, is equal to one.

2.2.5.2 The bCF approach has two parameter estimation options

Both parameter estimation options provide valid CF parameter and uncertainty estimates and will be described in the next two sections. Their primary difference is in how effect size is estimated and used. The user can select their preferred option based on the research question posed. To aid the reader, pseudocode for the MCMC procedure can be found in the Supplementary Materials (paragraph S2).

2.2.5.2.1 Parameter estimation option A

This option, referred to as bCF_A, closely replicates the standard CF approach and is computationally relatively 'light weight'. At each iteration, the CF parameters (σ,β) are estimated as follows. First, a predicted signal $p(t)$ is generated for CF position ($v_{o\ proposed}$) according to Eq. 2. Secondly, per time point, the error e_t between $p(t)$ and the measured signal $y(t)$ is calculated using an ordinary least squares fit (OLS) with free parameter β. Then, the log-likelihood L_t associated with e_t is estimated (Eq. 4). We assume that e_t follows a standard normal density function: $N(0,1)$. After estimating the mean and standard deviation of e ($\widehat{\mu_\epsilon}$ and $\widehat{\sigma_\epsilon}$), we calculate a maximum likelihood estimate (MLE). No thinning is applied to $\widehat{\sigma_\epsilon}$. In this option, only the prior for σ (l_σ; section 2.5.3) is used in calculating MLE (Eq. 5). Effect size β is not retained.

$$L_t = log(N(-|e_t|, \widehat{\mu_\epsilon}, \widehat{\sigma_\epsilon})) \quad 4)$$
$$MLE_A = \sum_t L_t + log\ (N(l_\sigma, 0, 1)) \quad (5)$$

Next, the MLE of the proposed parameter values ($MLE_{proposed}$) is compared to that of the accepted values ($MLE_{accepted}$) based on an Acceptance ratio score Ar (6).

$$Ar = exp\ (MLE_{proposed} - MLE_{accepted}) \quad (6)$$

Ar can be seen as a normally distributed pseudo-random acceptance score $N(0,1)$ and only if Ar is positive, the proposed parameter values become the accepted ones. Then, the next MCMC iteration takes place.

2.2.5.2.2 Parameter estimation option B

This option, referred to as bCF_B, primarily differs from bCF_A in that at each iteration, the MCMC procedure jointly estimates the CF parameters σ and β. Secondly, the priors for both σ and β (l_σ, l_β; section 2.5.3) are used in calculating the MLE (Eq. 7). Finally, β is retained for use in further analyses and thresholding (see paragraph 2.6.2).

$$MLE_B = \sum_t L_t + log(N(l_\sigma,0,1)) + log(N(l_\beta,-2,5)) \quad (7)$$

2.2.5.3 Proposing parameters using latent variables and priors

As already described in section 2.5.2, each iteration of the MCMC procedure, new values for the parameters of the CF model are proposed (referred to below with *proposed*) and, depending on the outcome of the Ar evaluation (Eq. 6), accepted (referred to below with *accepted*) or rejected. In this section, we describe how the proposed values are generated. Following Zeidman et al. (Zeidman et al. 2018), we use latent variables and corresponding transfer functions to relate these to the CF parameters. In order to obtain a likelihood on a model, it is beneficial to have (latent) parameters, e.g. l_σ, follow a gaussian distribution on the interval $-\infty$ and $+\infty$ (Eq. 5 and 7). At the same time, the transfer function can constrain the CF parameters to reflect prior knowledge.

2.2.5.3.1 Connective Field position

At each iteration, a new CF position ($v_{o\ proposed}$) is selected that is at a distance $step$ from the currently accepted CF center ($v_{o\ accepted}$). This distance $step$ ranges between 0 and a maximum possible stepsize [0 ms] (Eq. 8, Eq. 9). The maximum step size (ms) is defined as half the maximum distance in the matrix $D(v, v_o)$ (Eq. 8). To calculate $step$, a latent variable l_s is randomly drawn from a normal distribution N(0,1) and multiplied with maximum step size (ms), resulting in a flat prior for step size. The newly proposed CF position ($v_{o\ proposed}$) is set to the voxel in the source region with a distance to the current position that is as close as possible to $step$. If multiple positions are found, one of these is selected at random.

$$ms = max\ (D(v,v_{0\ accepted}))/2 \quad (8)$$
$$step = ms * NCDF(l_s, 0,1) \quad (9)$$

Note that on the first iteration, the CF center ($v_{0\ accepted}$) is set at the position of a random voxel in the source region. Based on the proposed and accepted CF centers respectively, two distance matrices $d_{proposed}$ (Eq. 10) and $d_{accepted}$ (Eq. 11) are derived.

$$d_{proposed} = D(v, v_{0\ proposed}) \quad (10)$$
$$d_{accepted} = D(v, v_{0\ accepted}) \quad (11)$$

2.2.5.3.2 Connective field size

Simultaneous with a newly proposed sample position, also a new CF size (σ) is proposed. For σ, its associated latent variable is l_σ. The prior for l_σ is defined by a normal distribution $N(0,1)$ (Eq. 12).

$$\sigma = (r - r_0) * NCDF(l_\sigma, 0, 1) + r_0 \quad (12)$$

$NCDF$ denotes the normal cumulative distribution function. Note that σ is constrained to the range $[r_0\ r]$, where r_0 is the minimum radius and r is the maximum radius for the CF (which are set to 0.01° and 10.5°, respectively). Note that r_0 can be set to any arbitrarily small non-zero number.

At each MCMC iteration, an $l_{\sigma\ proposed}$ is drawn from a normal probability density function N centered around the current value with a width of w (Eq. 13). Note that w has a fixed value of 2.

$$l_{\sigma\ proposed} = N(l_{\sigma\ accepted}, w) \quad (13)$$

2.2.5.3.3 Effect size

In the bCF_B , (section 2.5.2.2), β is estimated jointly with CF size and constrained to be positive (Zeidman et al. 2018) using the following equation:

$$\beta = exp(l_\beta) \quad (14)$$

The latent variable l_β is defined with a prior distribution $N(-2,5)$ and the proposed β value is controlled by $l_{\beta\ proposed}$ (Eq. 15).

$$l_{\beta\ proposed} = N(l_\beta, w) \quad (15)$$

The initial values of $l_{\sigma\ initial}$, $l_{\beta\ initial}$ and w are set to 1 , -5 and 2, respectively. As an aside, note that in bCF_A (section 2.5.2.1), β is estimated at a higher hierarchical level inside the loop using an OLS fit and can, theoretically, range between $-\infty$ and $+\infty$.

2.2.5.4 Alternative kernel: Difference of Gaussians

In addition to the single Gaussian (SG) model described above, we also implemented a Difference of Gaussian (DoG) model. The DoG model has previously been proposed for modeling surround suppression in stimulus-driven pRF models (Zeidman et al. 2018; Zuiderbaan, Harvey, and Dumoulin 2012). In the DoG model, the first Gaussian represents the center and is defined using the same parameters as in the SG model (i.e. ν_0, σ_1, and β_1). The second Gaussian of the DoG represents the surround suppression and uses the same position parameter as the SG, but is defined using independent parameters for size (σ_2) and amplitude (β_2). Size parameter σ_2 is constrained to be equal to or larger than σ_1 (Eq. 16). The amplitude β_2 is constrained to be negative and smaller than β_1 (Eq.17 and Eq. 18). This is enforced using two scaling parameters σ_d and β_d, for size and amplitude, respectively.

$$\sigma_2 = \sigma_1+\sigma_d \quad (16)$$

$$\beta_2 = max\,(\beta_1-\beta_d,0) \quad (17)$$

$$P_{DoG}(t) = p_1(t)\beta_1-p_2(t)\beta_2 \quad (18)$$

Parameter σ_d is constrained to be between $[0,r_d]$(see Eq. 12) using a latent variable $l_{\sigma 2}$ which is defined according to a standard normal distribution N(0,1) (see Eq. 13). r_d is the largest allowed difference in radius for the second Gaussian compared to the first and is set to 0.5°. This means that the initial value of σ_2 can be between 0 and 0.5 deg larger than that of σ_1. The β_d was forced to be positive (Zeidman et al. 2018) with a latent variable $l_{\beta 2}$ with a prior distribution $N(-2,5)$ (see Eq. 15).

In this study, when estimating the DoG model, we used bCF_B in which all β_1 and β_2 values and their associated probabilities are retained for further analysis. The initial values of $l_{\sigma 2\ initial}$ and $l_{\beta 2\ initial}$ were set to 5 and 10, respectively. The DoG implementation for bCF_A is described in the supplementary material.

2.2.5.5 Model validation and comparison

For each participant, the sCF and both bCF estimation options were applied taking V1 as the source region that is sampled by various target regions (V2,V3,hV4, LO1 and LO2). Target and source regions were defined as described in section 2.4.2. When validating the output of the sCF and bCF_A models, we thresholded on variance explained (Haak, Morland, and Cornelissen 2013). Only voxels for which the best-fitting CF model explained at least 15% of the time-series variance were included. The more principled thresholding approach applied in bCF_B is described below in section 2.6.2. To quantify the level of agreement between the sCF and either of the bCF options, the estimates for the CF parameters (position and size) for each target region are compared using Pearson correlations at both the participant and the group

level. Correlation values higher than 0.5 and p-values below 0.05 were considered statistically significant. Furthermore, a family-wise error corrected (FWE) permutation test was used to determine wherever differences based on the VE parameter between SG and DoG models were significant. The permuted labels were repeated 1000 times per subject, $p \leq 0.05$ was considered statistically significant.

2.2.6 Bayesian analysis and new model features

2.2.6.1 Uncertainty

Based on a quantile analysis of the estimated posterior distribution, we computed a voxel-wise uncertainty measure (Papadopoulos and Yeung 2001) for the bCF parameters estimates as follows:

$$U = Q_3 - Q_1 \tag{17}$$

Where Q_3 and Q_1 represent the upper and lower quantiles of the posterior distribution, respectively. Furthermore, we computed the cross-correlation coefficients to quantify possible dependencies between the bCF parameters (VE, *sigma* and *beta*; the latter only for bCF_B) and their associated uncertainties. For each target region, these correlations were computed at both the participant and the group level.

2.2.6.2 Beta thresholding

In fMRI research, it is generally considered good practice to limit analysis of the parameter estimates to voxels with reliable model fits. In the pRF literature, this is commonly done by setting a variance explained threshold (typically fixed at 15%). A more principled approach would be to verify whether the probability of an estimated model effect size is larger than may be expected on the basis of chance alone. As such, the estimated values must be compared against their null-distribution. Often, this null-distribution can be derived from theoretical considerations (e.g. t-distributions) and estimates of the degrees of freedom of the model (parametric approach). However, due to both spatial and temporal dependencies in the data, it is generally preferred to construct an empirical null-distribution by sampling the model estimations using randomly generated data with a spatiotemporal covariance structure that is similar to that of the real data (non-parametric approach).

In this context, a second consideration pertains to the statistic upon which thresholding will be based. Intuitively, the overall model fit is quantified by the total amount of variance that is explained by the model. The threshold criterion can then be chosen such that this quantity is significantly greater than zero (e.g. the quantity falls within the 95th percentile of the null distribution). When the model involves just a single free scaling parameter (i.e. effect size), testing whether this scaling is greater than zero

is often equivalent to testing the significance of the overall model fit (i.e. variance explained). This is the case in standard pRF and CF modelling as well as in bCF_A. There, a candidate model prediction is iteratively generated and the goodness of fit is determined using a single scaling parameter (eq. 1). However, in bCF_B, the scaling parameter beta is jointly estimated with sigma. Thresholding by testing whether beta is greater than zero may therefore yield different results compared to thresholding based on variance explained. This is due to potential dependencies between beta and sigma. In the case of a joint estimation, the parameter beta can be interpreted as a form of response gain (summarizing the combined effects of the neuronal and BOLD response gains). Therefore, in bCF_B, testing the significance of beta provides an alternative for thresholding. This more directly addresses the question of whether or not the activity of a voxel in the target region is meaningfully associated to that in the source region.

In order to use beta as a data-driven threshold, a proxy distribution for the null hypothesis (which states that there is no correlation between the source and target region) is required. We calculate this null distribution based on surrogate BOLD time series. To do so, for each voxel in the target region, surrogate BOLD time series were generated from its actual BOLD time series using the iterative Amplitude Adjusted Fourier Transform method (iAAFT) (Räth and Monetti 2009; Schreiber and Schmitz 1996). This method removes any temporal correlations between voxels within the target region. Then, the bCF_B model is fitted to the surrogate time series of the target voxel and the real BOLD time series of the source region.

For the thresholding, we have implemented two variants: a beta-uncorrected and a beta-corrected threshold. Figure 2 provides an overview of both. The beta-uncorrected threshold is determined independently for each voxel in the target region. The bCF_B model is fitted to a total of 40 surrogate time series generated for the voxel (this number was chosen for no other reason than computational feasibility). In this case, the null distribution is the aggregate of all the betas estimated at voxel level by calculating the 95th percentile of this distribution, a voxel-specific beta-uncorrected threshold is obtained. In case of the beta-corrected threshold, the posterior null distribution is the aggregate of the betas estimated for all voxels in the target region. The beta-threshold is the 95th percentile of this aggregated null distribution. In this way, the *beta*-threshold is familywise error (FWE) corrected for all the voxels in the target region. While in regular use a single aggregate distribution will be sufficient, in the present study, we generated 40 aggregate null distributions for the target region. These were used to verify the appropriateness of the *beta*-corrected threshold variant. One of these distributions was selected at random and used to determine the beta threshold.

To quantify the usefulness of these new thresholding approaches and that of the standard VE thresholding were compared using surrogate and real time series at the participant level.

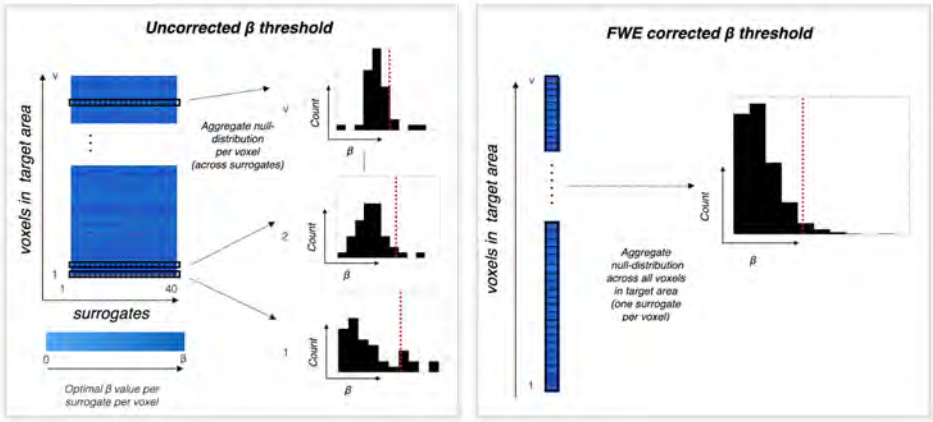

Figure 2 - Illustration of the two beta thresholding options available during Bayesian CF modeling. For each voxel in the target region, a null distribution for beta is estimated based on surrogate BOLD time series. The resulting optimal fits for a sample of 40 voxels, is presented in the voxel-by-surrogate matrix (left hand side). The bCF_B has two options for thresholding based on *beta*. Left: when selecting the "uncorrected threshold" option, an optimal threshold for beta is computed for each individual voxel in the target region. The *beta*-threshold is based on the 95th percentile of the null distribution for that particular voxel (indicated by the red line in each of the histograms). Consequently, the optimal *beta*-threshold will be specific to each voxel. Right: when selecting the "FWE-corrected threshold" option, the optimal *beta*-threshold is based on the 95th percentile of the aggregate null distributions of all voxels in the target region.

2.2.6.3 Model selection

To compare the SG and DoG models, three parameters were considered: the variance explained (VE) of the model, the Bayesian Information Criterion (BIC, see Eq. 18) (Schwarz 1978; Myung and Pitt 2004) and Akaike's Information Criterion (AIC, Eq. 19).

$$BIC = ln(n) * k - 2 * ln(MLE) \quad (18)$$

$$AIC = 2 * k - 2 * ln(MLE) \quad (19)$$

Where n is the number of time series (in our study set to 124) and k is the number of free model parameters (set to 2 and 4 for the SG and DoG models, respectively). Per target voxel, the best model was determined based on having either the lowest BIC value, the lowest AIC value, or the highest VE.

2.3 RESULTS

To preview our results, we observe a good level of agreement between the sCF and the bCF models. We estimated the uncertainty and (in)dependence of the bCF parameters (σ and β). Moreover, we show the effect of thresholding based on the model's effect size. Finally, we found that a CF model based on a single Gaussian was preferred over one based on a DoG to explain the observed BOLD correlations between visual areas.

2.3.1 Standard and bCF models provide similar CF estimates

Figure 3 shows the bCF_A and the sCF estimates plotted on a smoothed 3D cortical surface of a representative participant. The maps were obtained using V1 as the source and V2, V3, hV4, LO1 and LO2 as the target regions. The maps for both methods show a clear visuotopic organization for all the CF parameters estimated and are in good agreement (Figure 3, panels a and b). Furthermore, figure 4 illustrates the generally high levels of correlation between the sCF and the bCF_A model estimates at the voxel level for this participant. Specifically, panels a and b indicate that the coverage of the visual field is similar between the two methods. Furthermore, panel c indicates that the same is true for the CF size. Some exceptions to this general finding are, presumably, due to low voxel counts (e.g. eccentricity in LO2, CF size in hV4).

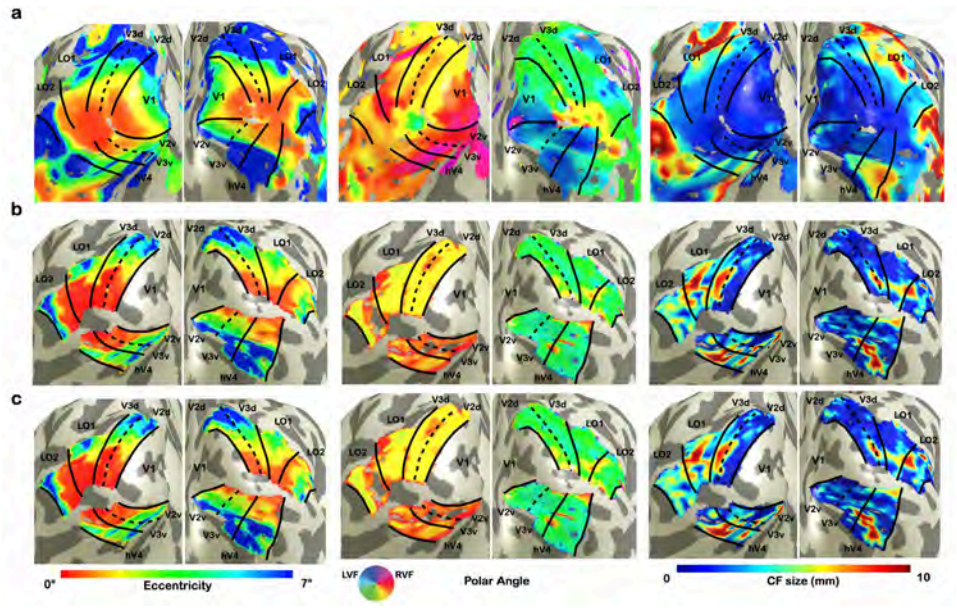

Figure 3 - The Bayesian CF reproduces the basic parameters of the standard CF approach. Panels a: maps for eccentricity, polar angle and CF size based on bCF_A; Panels b: reference maps based on sCF; Row c: reference retinotopic and CF size maps based on pRF mapping. The left (eccentricity) and middle (polar angle) panels of row a and b show retinotopic maps reconstructed

via CF models, using V1 as the source. Borders between visual areas are indicated by black lines. All maps are for a single participant. Supplementary Figure S1 shows the corresponding maps for bCF_B of this participant. Figure 4 shows the voxel level correlations between the sCF and bCF results of this participant.

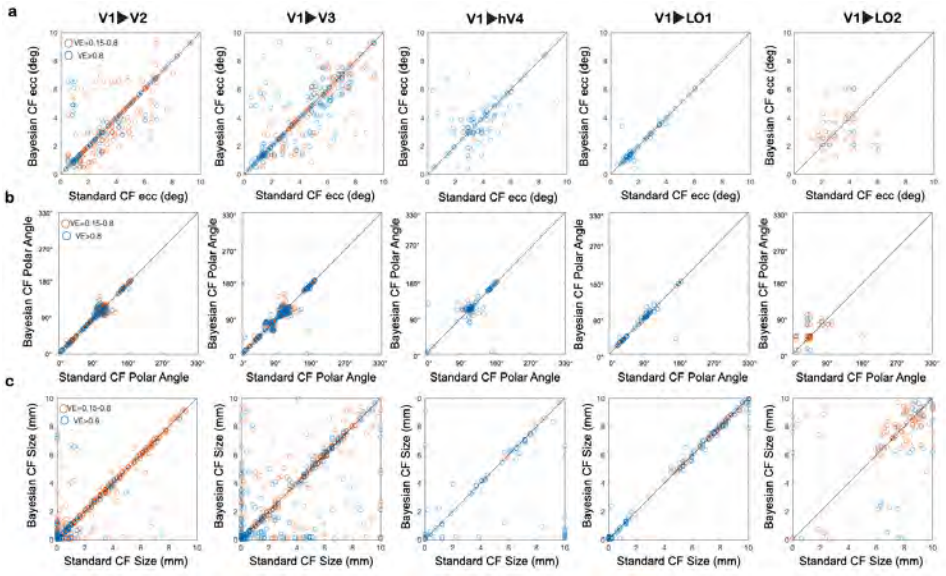

Figure 4 - Voxel level correlations between the results of the standard CF and Bayesian CF. Results are for the participant shown in Figure 3. Columns from left to right show the CF estimates for the target regions V2, V3, hV4, LO1 and LO2, each of them sampling from source region V1. Panels **a**, **b** and **c** show the (Pearson) correlations for eccentricity and polar angle (both converted into visual field coordinates) and CF size, respectively. Only voxels with a VE > 0.15 for the sCF model fit are considered. Voxel data points are color coded based on their VE: orange indicates a VE in the range 0.15-0.8 while blue indicates a VE higher than 0.8. Pearson correlation coefficients are reported. Correlation values for other participants are reported in the Supplementary Materials (Table S1).

Table 2 lists the group-level correlations for the eccentricity and polar angle maps reconstructed on the basis of the sCF and both bCF model outputs with those derived directly using pRF mapping (which serves as the gold standard).

Overall, we observed good levels of agreement between the outputs of the sCF and bCF frameworks. This indicates that bCF accurately estimates the cortico-cortical properties of the human visual cortex. Correlation values obtained at the single level are reported in the supplementary material (Table S1). Additionally, we provide an example comparison between the beta estimates obtained using the bCF_A and the bCF_B models (Supplementary Figure S3).

Table 2 - Group level (median) correlations between visual field map parameters derived from pRF, standard CF and both Bayesian CF models.

Eccentricity									
ROIs	*Standard CF*			*bCFa*			*bCFb*		
	rho	*IQR[Q1,Q3]*	*p-value*	*rho*	*IQR[Q1,Q3]*	*p-value*	*rho*	*IQR[Q1,Q3]*	*p-value*
V1 --> V2	0.8681	[0.822,0.905]	p<0.001	0.8653	[0.819,0.905]	p<0.001	0.8728	[0.814,0.899]	p<0.001
V1 --> V3	0.8254	[0.783,0.874]	p<0.001	0.8239	[0.775,0.873]	p<0.001	0.8222	[0.763,0.865]	p<0.001
V1 -> hV4	0.8094	[0.73,0.838]	p<0.001	0.7911	[0.731,0.837]	p<0.001	0.7884	[0.711,0.837]	p<0.001
V1 -> LO1	0.78	[0.724,0.816]	p<0.001	0.7811	[0.717,0.819]	p<0.001	0.791	[0.7204,0.823]	p<0.001
V1 -> LO2	0.705	[0.595,0.816]	0.002	0.6566	[0.538,0.759]	0.0045	0.6616	[0.462,0.731]	0.0015
Polar Angle									
ROIs	*Standard CF*			*bCFa*			*bCFb*		
	theta	*IQR[Q1,Q3]*	*p-value*	*theta*	*IQR[Q1,Q3]*	*p-value*	*theta*	*IQR[Q1,Q3]*	*p-value*
V1 --> V2	0.9178	[0.844,0.929]	p<0.001	0.918	[0.870,0.929]	p<0.001	0.9142	[0.854,0.936]	p<0.001
V1 --> V3	0.8341	[0.744,0.916]	p<0.001	0.8429	[0.703,0.916]	p<0.001	0.8538	[0.713,0.927]	p<0.001
V1 -> hV4	0.7999	[0.524,0.920]	p<0.001	0.7959	[0.513,0.918]	p<0.001	0.8324	[0.497,0.921]	p<0.001
V1 -> LO1	0.8122	[0.554,0.902]	p<0.001	0.8257	[0.553, 0.9]	p<0.001	0.8101	[0.567, 0.896]	p<0.001
V1 -> LO2	0.7226	[0.515,0.833]	0.003	0.6755	[0.512, 0.817]	0.001	0.6491	[0.426, 0.842]	0.003

Correlation coefficients indicate the level of agreement in the eccentricity (*rho,* Spearman's correlations) and polar angle (*theta*, circular correlations) maps for the standard CF and both Bayesian CF models with the ones directly derived by pRF mapping *(*gold standard). Correlation and p-values were first estimated at the participant level and then concatenated across all participants to determine the median and interquartile range (IQR). The correlation values for each participant are reported in the Supplementary Materials (Table S1).

2.3.2 Results of new Bayesian CF functionality

2.3.2.1 Uncertainty

An important theoretical advantage of the Bayesian approach is that, besides the optimal values of the CF parameters (σ,β,VE), it also determines their associated (posterior) uncertainty.

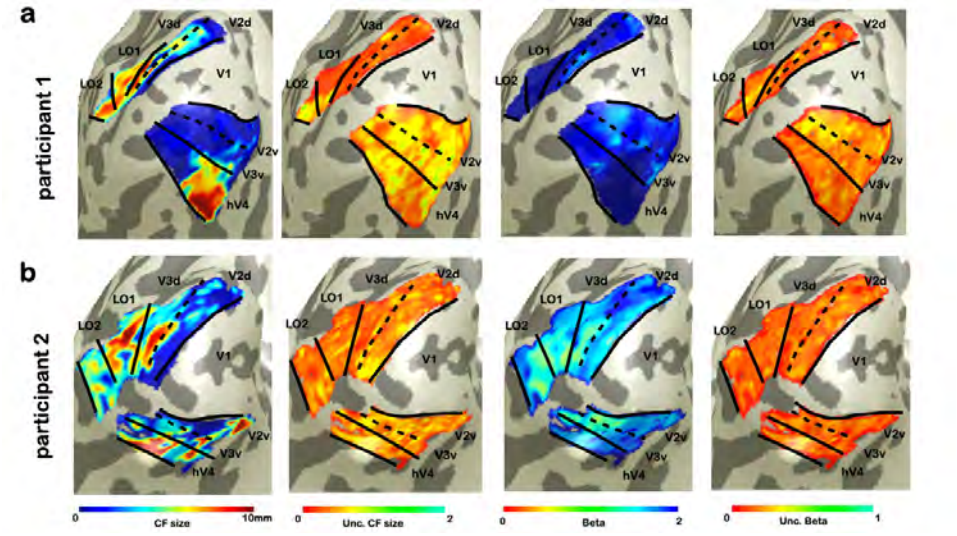

Figure 5 - Illustrative visualization of CF size and beta and their associated uncertainties as estimated using bCF$_b$ for two participants. From left to right: CF size, uncertainty of CF size, beta and uncertainty of beta. Panel **a** and **b** show these bCF parameters obtained for two participants. For further illustration, Figure 6 plots the uncertainties for V1>V2 for these two participants as a function of eccentricity.

For illustrative purposes only, Figure 5 shows the cortical projections of CF size and beta as well as their associated uncertainties for V1>V2 for two participants. Again for illustrative purposes, Figure 6 shows the uncertainty estimates of these same two participants as a function of (pRF-derived) eccentricity.

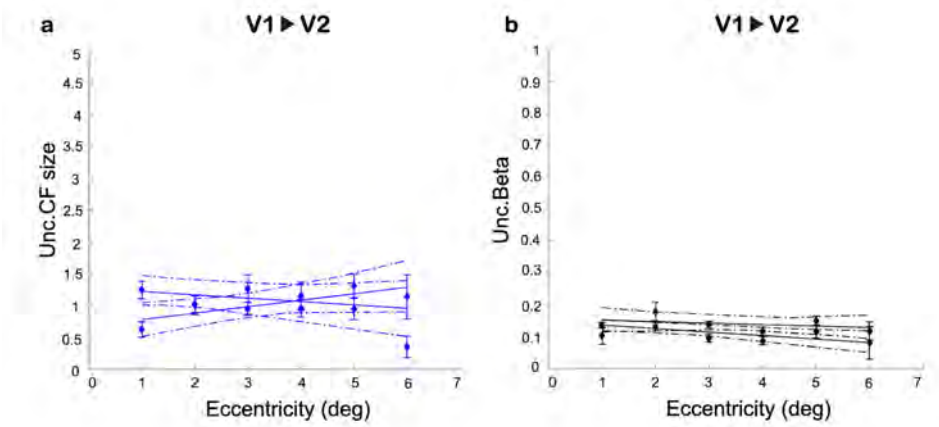

Figure 6 - Illustration of the uncertainties for CF size and beta as a function of pRF-based eccentricity of V1>V2 for two participants. Panels **a** and **b** show the relation between eccentricity and uncertainty associated with CF size and beta, respectively. Eccentricity was binned in intervals of 1 deg and a linear fit was applied. The average derived uncertainty was calculated only for voxels with a variance explained > 0.15. Each dot indicates the mean of the uncertainty in each bin. The dashed lines correspond to the 95% bootstrap confidence interval of the linear fit. Participants are the same as those shown in Figure 5.

Figure 7 shows the cross-correlation coefficients between the MCMC parameters, the corresponding (posterior) uncertainties and the residual noise. For all target ROIs, VE and the uncertainties for σ and β are moderately and negatively correlated. The bCF parameters are only weakly correlated with their corresponding uncertainties.

2.3.2.2 Beta thresholding

The bCF_B enables to test whether or not the activity of a voxel in the target region is meaningfully associated to that in the source region, based on the distribution of *beta* (see section 2.6.2). For illustration purposes, figure 8 shows the distribution of β values estimated for a single V2 target voxel based on either its real (panel 8a) or a surrogate (panel 8b) time-series. The dotted line in panel 8a indicates the optimal estimate. Panel 8c shows the null distribution of beta over 40 surrogate times series for this voxel. Based on the 95th percentile of the beta distribution over surrogates, a *beta*-uncorrected threshold can be defined for this voxel. Panel 8d shows 10 examples of

null distributions of beta aggregated over all V2 voxels (each distribution is shown at a different gray level). It is clear that these aggregate distributions are highly comparable and will also result in very similar FWE-corrected beta thresholds.

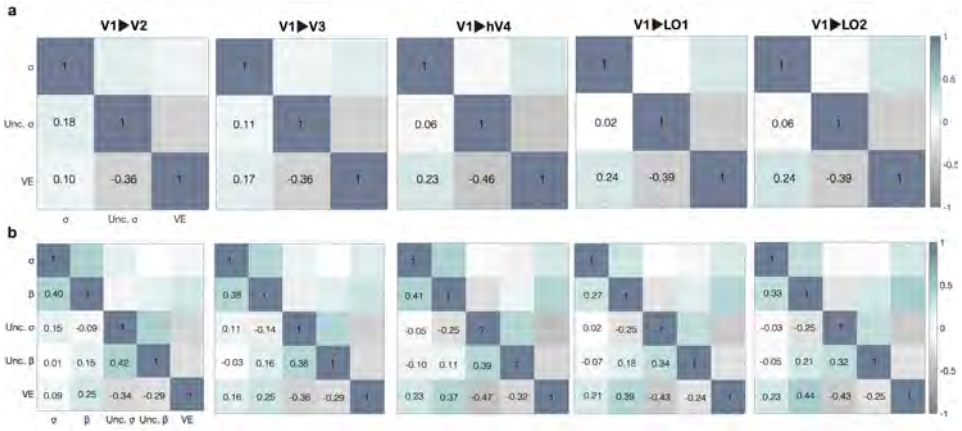

Figure 7 - Cross correlations between bCF parameters and their associated uncertainties at the voxel level. Panels **a** and **b** show the correlations obtained using bCF_A and bCF_B, respectively. Only the CF parameters directly estimated using the model (σ,β and VE) are included in this analysis. The bCF parameter values and their associated uncertainties were first estimated at the participant level and then concatenated across all participants to determine the medians. Boxplots of the statistical dependencies between the bCF parameters and their uncertainties at the individual level are shown in supplementary Figures S2 and S3.

2.3.4 Model comparison

The bCF also enables model comparisons at the voxel level that take the number of free parameters into account. Here, we use the likelihood estimations of the bCF_B (see sections 2.5) to calculate Bayesian Information Criterion (BIC) and Akaike's Information Criterion (AIC) scores and compare whether SG or DoG models better explain the responses of the target voxels. For both criteria, lower values indicate more evidence for a particular model. Figure 9, panels b and c show that on average, in all visual areas, the voxels have only slightly lower BIC and AIC scores for the SG compared to the DoG. Panels 9d and 9e show that when plotted in terms of their preferred model, the voxels of all areas predominantly prefer the SG model. For comparison, we also compare the fits of the SG and DoG models using VE (Figure 9a). A slightly higher VE is found for the DoG compared to the SG model across all visual areas but these differences are not significant (p-values range from 0.64 to 0.28). Finally, figures 9f and g show, for a single hemisphere of one participant, the BIC values for all voxels projected onto the smoothed cortical surface. Figure 9h shows the difference between the BIC scores of the SG and DoG models. No clear visuotopic organization seems to be present.

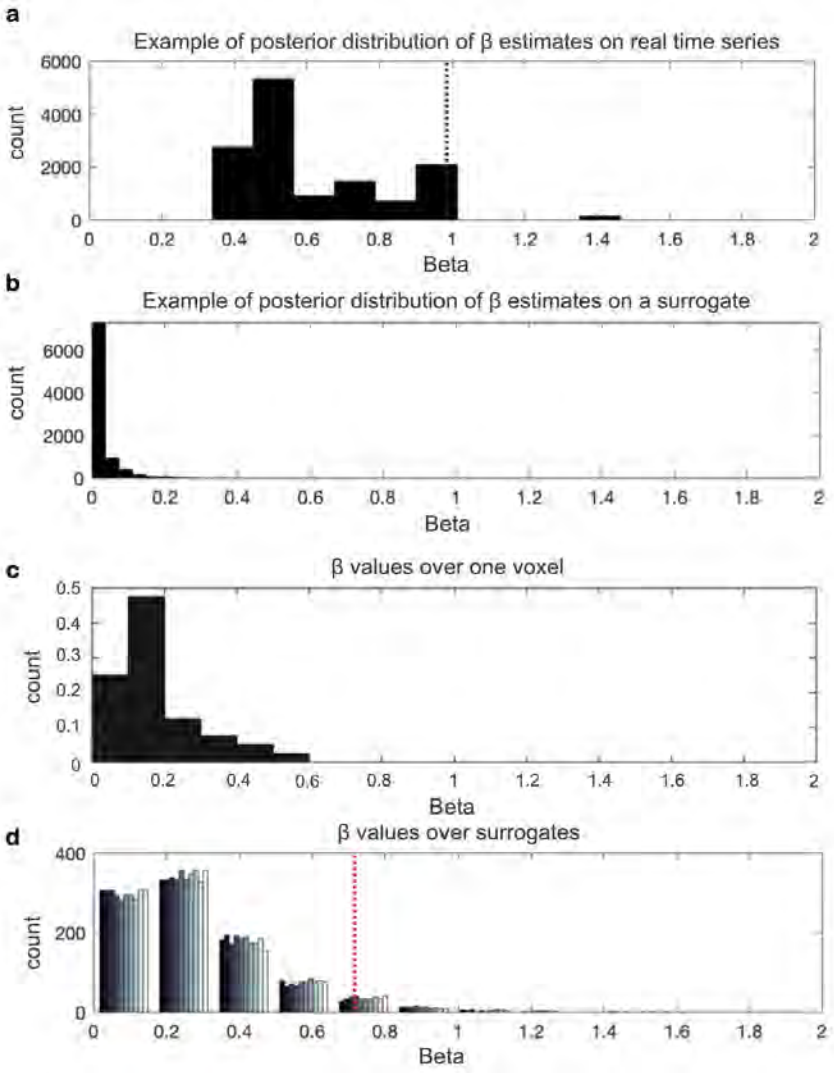

Figure 8 - Illustration of the *beta*-based threshold distributions and estimates. In panels **a** and **b**, the histograms show the posterior distribution of beta for a single target voxel in area V2 (sampling from V1) for a real and surrogate time series, respectively. In panel **a,** the best fitting bCF beta estimate for this voxel (β= 0.98) is indicated by the black dotted line. Panel **c** shows the histogram of the best fitting beta over one voxel. This histogram can be used to obtain an uncorrected threshold. Finally, in panel **d**, each gray bar shows the distribution of best fitting beta values under the null hypothesis (i.e. surrogate data) across all voxels in V2. Each bar represents a distribution based on one surrogate. For comparison purposes only, we present 10 aggregate distributions. The red dotted line indicates the FWE-corrected beta threshold (β= 0.72) for one (randomly selected) distribution. A comparison of the beta estimates for both bCF options is reported in supplementary Figure S3.

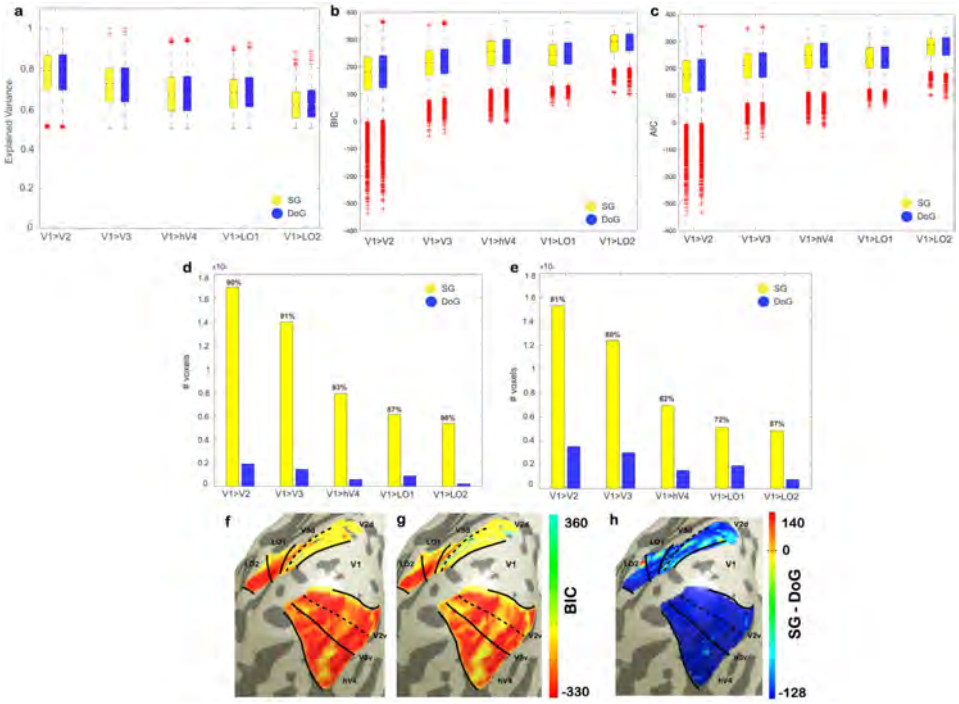

Figure 9 - Model comparison between SG and DoG bCF models. Variance explained and BIC were computed at the single subject level and then averaged over the population per ROI for both the SG and DoG bCF models. Data was thresholded using the confidence interval (CI) corrected *beta*-based option. Panels **a,b and c** show for both models the Explained Variance , BIC and AIC scores, respectively. For almost all ROIs, the DoG CF model (blue) has a larger VE compared to SG CF model (yellow). Panels **d and e** show per ROI the number of voxels with a lower BIC or lower AIC, respectively. The percentage is provided on top of each bar for the SG model In all ROIs, the simpler model is favored when the number of model parameters is taken into account. Panels **f** and **g** show, for a single participant, the projections of the BIC values onto a smoothed cortical surface for the SG and DoG CF models, respectively. Panel **h** shows, for the same participant, the projections of the BIC difference between for two CF models (SG - DoG), with more negative values indicating greater evidence for the SG model.

2.4 DISCUSSION

In the present work, we show how a Bayesian variant of the CF modeling approach can be used for a detailed assessment of the cortico-cortical properties of the visual system. Importantly, the parameter estimates of the bCF agree with those of the sCF while additionally providing the uncertainties associated with the voxel-level estimates of CF size and effect size (β). Finally, we find that for the majority of voxels in the early visual cortex, a SG is prefered over a DoG model. This suggests that CFs do not possess a center-surround organization. Below, we discuss our results in more detail.

2.4.1 The Bayesian inference approach accurately characterises cortico-cortical receptive field properties

We find that the Bayesian Connective Field output compares well to that of the standard approach.

The visuotopic maps based on the bCF are qualitatively similar to those based on the sCF (Figure 3). When quantified, the highest degree of similarity between bCF and sCF was observed for V1 projecting to V2 (V1>V2) and V1 projecting to V3 (V1>V3). These quantitative and qualitative results are in agreement with those presented previously (Haak V. et al. 2013). This high degree of correspondence indicates that the Bayesian inference approach provides the same parameter estimates while providing new information: the underlying posterior distributions and the uncertainty associated with each parameter.

In the past years, Bayesian approaches have been applied to the pRF method allowing estimation of the full posterior distribution associated with each of the receptive field properties (Zeidman et al. 2018; Quax et al., n.d.; Adaszewski et al. 2018; Benson and Winawer 2018; Carvalho et al. 2020). Similar to these Bayesian pRF methods, the Bayesian CF framework now provides the full posterior distribution associated with each of the cortico-cortical model parameters. From this, parameter uncertainty can be derived and possible dependencies between parameter estimates can be quantified. Importantly, we find that the uncertainty estimates do not correlate with the parameter estimates themselves (see Figure 7). At most weak correlations were observed between the bCF parameters and their corresponding uncertainties (with correlations mostly below 0.25). Therefore, the uncertainties can be treated as additional, independent CF parameters to quantify reliability. A moderately strong inverse relationship was observed between the goodness of fit of the model (VE) and the uncertainties. While this might suggest the uncertainties do not provide additional information on the data, in the next section we will show they do, nevertheless. The uncertainty may be used in various ways to increase confidence in the CF model predictions. For example, it may be used for statistical comparisons at the level of single individuals, which can be important in the context of patient studies, in particular when assessing rare cases, where group averages are not available. Moreover in patient studies, it will help to quantify the reliability of the estimates in each patient (see Chapter 4). As we will discuss later, it can also be used to test different models at the single voxel level.

2.4.2 The effect size provides a data driven threshold

The standard and widely used approach to select the most reliable voxels uses thresholding based on the goodness of fit of the CF model (i.e. on VE) (Haak, Morland, and Cornelissen 2013; Halbertsma, Haak, and Cornelissen 2019). However, a high VE

does not necessarily correspond with a low variability in the estimates (Thielen et al., n.d.). In fact, a model fitted to noisy data may still get a high VE. Based on the Bayes CF framework, we developed two thresholding techniques based on the posterior distributions of effect size β: 1) an uncorrected threshold per voxel and 2) a threshold, FWE corrected for all voxels in a target ROI.

The suitability and gain of these new threshold options depends on the goals of a study. In general, the FWE-corrected *beta*-threshold provides the most conservative threshold (Chapter 3). Critically, the new thresholds are data-driven and thus participant- and even area- or voxel-specific. Therefore, we expect that these *beta*-thresholds will be particularly useful when bCF modeling is applied in clinical populations (e.g with a lesioned visual pathway or cortical neurodegeneration). Deriving these *beta*-thresholds requires the generation of a proxy distribution for the null hypothesis based on surrogate BOLD time series. At present, obtaining voxel-specific thresholds is computationally demanding or time consuming. This is less so for the FWE corrected threshold where a single surrogate BOLD time series per voxel will suffice. We verified this by generating 40 surrogate null-distributions across the voxels of an area which turned out to be highly consistent (see Figure 8d).

2.4.3 Connective fields do not possess a spatial center-surround structure

Another functionality gained through the bCF is the ability to compare different cortical receptive field models at the voxel level. In pRF modelling, an larger VE was reported for a Difference of Gaussian (DoG) pRF model compared to a single Gaussian (SG) model in the early visual cortical areas (Zuiderbaan, Harvey, and Dumoulin 2012; Zeidman et al. 2018). Therefore, a DoG pRF model may better explain the observed fMRI signal in early visual cortex. Moreover, being able to assess this feature is useful, as center-surround configurations of pRFs may be different in clinical populations (Anderson et al. 2017; Zhang, Abbey, and Eckstein 2009; Grigorescu, Petkov, and Westenberg 2003).

To illustrate the new bCF functionality, we compared a SG CF model to a DoG CF model on the basis of VE, AIC and BIC values. On average, a slightly larger but non-significant difference in VE was observed for the DoG compared to the SG CF models in all the visual cortical areas (see Figure 9). However, a priori a higher VE for the DoG is expected due to its additional degrees of freedom (4 rather than 2 for the SG) (Haefner and Cumming 2008; Singh and Horn 1999). This complicates model comparison at the voxel level. In contrast, AIC and BIC scores do take model complexity into account. On average, the differences between the SG and DoG scores were very small. Nevertheless, on the basis of either score, the majority of the voxels (~ 80%) in all visual areas preferred the SG model. This indicates that the more complex DoG model may

overfit the data. Therefore, we conclude that unlike pRFs, cortico-cortical interactions as modeled using the CF do not require a spatial center-surround organisation.

2.4.4 Limitations

In analogy to the standard CF model, we forced the CF center (i.e. center of the gaussian kernel) to coincide with a voxel in the source region. Moreover, in the MCMC procedure, the distance of the accepted CF center to other voxels is computed by using Dijkstra's algorithm (Dijkstra 1959); as implemented in the mrVista environment). Thus, the CF location/center is discrete since distance is based on the vertices of a mesh. This may result in an 'edge effect' as the model cannot sample outside of the source region. In particular, near the edges of the source region this may influence the symmetry in the chosen step updates which, in turn, may cause an asymmetry bias in the sampled locations. Note that we did not observe such an effect in our visual field reconstruction. Although location sampling may be biased near the edges, this will have only minimal impact on our results as we only use the "optimal-fit location" for further analysis.

Compared to the sCF, the bCF framework is computationally demanding. Currently, we addressed this by using parallel GPU computing and implementing the method using cluster computing (https://wiki.hpc.rug.nl/peregrine/start) - per node, we used 48 Intel Xeon 2.5 GHz cores with 512 GB of internal memory (Avesani et al. 2019). We employed 17500 iterations and removed 10% to account for bleed in. This provided a decent sampling of the posterior distribution in a reasonable amount of time (~ 21h per visual area). Future advances in hardware and software optimization will contribute to reducing the computation time. Furthermore, a thinning procedure to reduce the memory demand may be considered.

Thus far, when comparing models, possible autocorrelations in the time courses of the source region, as well as possible covariations between parameter estimates during the MCMC iteration process have not been accounted for. The first point may result in an overestimation of the effective number of points (degree of freedom) which will impose an additional penalty when adding parameters to the model. The second point may overestimate the number of independent/free parameters, again posing a (possible) additional penalty on increasing the number of parameters. Taken together, the model comparison that we have performed thus far, is bound to be conservative, i.e. it will tend to favour the model with fewer parameters.

2.4.5 Future directions

The bCF presented here uses a straightforward biological-grounded model to assess the cortical receptive field properties, and provides a starting point for future studies. Similar to the sCF model, the bCF model is stimulus-agnostic. Previous studies have

shown that the sCF still reflects the visuotopic organization of the visual cortex when applied to BOLD activity recorded in the absence of external stimulation (i.e. resting-state fMRI data) (Gravel et al. 2014; Bock et al. 2015). In a similar way, the bCF model will be able to extract connectivity based on intrinsic activity. Thus, it may be used to evaluate the quality of cortical processing in participants in which the visual input may be compromised by ocular or neurological lesions (Carvalho, Renken, and Cornelissen 2019).

The bCF may allow better monitoring of disease progression or the effect of an intervention. Beta and the associated uncertainty can be used to rate data and model fit quality in individual participants. Moreover, the uncertainty associated with other parameters can be used to weight the contribution of a participant to a group average. This may improve our insights into the cortical components of neurological or neuro-ophthalmic diseases, such as e.g. glaucoma or Parkinson's disease.

Future implementations of the code should incorporate methods to account for (possible) autocorrelations in the time series of the source, as well as covarying parameter estimates during the MCMC iteration process. For example, the first issue may be ameliorated by implementing a "thinning" procedure, whereas the covariance between parameters can be estimated from the MCMC iterations. This may provide further insight in the interdepencies introduced by the model which may affect efficient estimation.

The bCF framework allows to compare different model definitions which may provide novel information to characterize inhibitory cortical mechanisms in neuro-ophthalmic patients. Besides with a DoG model, the bCF may be extended with further model definitions that may characterize additional properties of the cortical interactions between visual areas (i.e. elongated shape, oriented ellipse, polar Gaussian, and the Cartesian and Polar Log-Gaussian (Kumano and Uka 2010; Zeidman et al. 2018). Furthermore, the bCF framework enables proper cortical model comparison by estimating the likelihood of a model. This allows to implement further Bayesian model selection using various criteria such as Bayes Factor or Free Energy (Penny 2012; Edwards, de Abreu, and Labouriau 2010). Being available at the voxel level, such criteria may be projected onto the cortical surface (or other representations) to investigate possible visuotopic (re-)organization.

2.5 CONCLUSION

In this study, we have presented and validated a Bayesian inference framework for CF modeling that is based on a Markov Chain Monte Carlo approach. When applied to empirical stimulus-driven fMRI data, we observed good agreement of the bCF and the sCF outputs.

The bCF approach has enabled various new functionality. First, it quantifies the parameter uncertainty associated with the CF parameters which may be used in various ways to increase confidence in the parameter estimates. Second, the effect size of the BOLD fluctuation (beta*)* can now be used to derive a reliable, data-driven threshold. Third, it enables voxel level comparison of different CF kernels. We find that a SG model suffices for describing the cortico-cortical interactions in the early human visual system. We conclude that our Bayesian CF framework provides a versatile tool to study the properties of the cortical interactive processes underlying perception, attention and cognition in health, development, aging and disease.

REFERENCES

Adaszewski, Stanisław, David Slater, Lester Melie-Garcia, Bogdan Draganski, and Piotr Bogorodzki. 2018. "Simultaneous Estimation of Population Receptive Field and Hemodynamic Parameters from Single Point BOLD Responses Using Metropolis-Hastings Sampling." *NeuroImage* 172 (May): 175–93.

Ahmadi, Khazar, Anne Herbik, Markus Wagner, Martin Kanowski, Hagen Thieme, and Michael B. Hoffmann. 2019. "Population Receptive Field and Connectivity Properties of the Early Visual Cortex in Human Albinism." *NeuroImage* 202 (November): 116105.

Anderson, Elaine J., Marc S. Tibber, D. Sam Schwarzkopf, Sukhwinder S. Shergill, Emilio Fernandez-Egea, Geraint Rees, and Steven C. Dakin. 2017. "Visual Population Receptive Fields in People with Schizophrenia Have Reduced Inhibitory Surrounds." *The Journal of Neuroscience: The Official Journal of the Society for Neuroscience* 37 (6): 1546–56.

Avesani, Paolo, Brent McPherson, Soichi Hayashi, Cesar F. Caiafa, Robert Henschel, Eleftherios Garyfallidis, Lindsey Kitchell, et al. 2019. "The Open Diffusion Data Derivatives, Brain Data Upcycling via Integrated Publishing of Derivatives and Reproducible Open Cloud Services." *Scientific Data* 6 (1): 69.

Benson, Noah C., and Jonathan Winawer. 2018. "Bayesian Analysis of Retinotopic Maps." *eLife* 7 (December). https://doi.org/10.7554/eLife.40224.

Bock, Andrew S., Paola Binda, Noah C. Benson, Holly Bridge, Kate E. Watkins, and Ione Fine. 2015. "Resting-State Retinotopic Organization in the Absence of Retinal Input and Visual Experience." *The Journal of Neuroscience: The Official Journal of the Society for Neuroscience* 35 (36): 12366–82.

Brainard, D. H. 1997. "The Psychophysics Toolbox." *Spatial Vision* 10 (4): 433–36.

Carvalho, Joana, Azzurra Invernizzi, Khazar Ahmadi, Michael B. Hoffmann, Remco J. Renken, and Frans W. Cornelissen. 2020. "Micro-Probing Enables Fine-Grained Mapping of Neuronal Populations Using fMRI." *NeuroImage* 209 (April): 116423.

Carvalho, Joana, Remco J. Renken, and Frans W. Cornelissen. 2019. "Studying Cortical Plasticity in Ophthalmic and Neurological Disorders: From Stimulus-Driven to Cortical Circuitry Modeling Approaches." *Neural Plasticity* 2019 (November): 2724101.

Chib, Siddhartha. 2011. "Introduction to Simulation and MCMC Methods." *The Oxford Handbook of Bayesian Econometrics*. https://doi.org/10.1093/oxfordhb/9780199559084.013.0006.

De Best, Pieter B., Noa Raz, Nitzan Guy, Tamir Ben-Hur, Serge O. Dumoulin, Yoni Pertzov, and Netta Levin. 2019. "Role of Population Receptive Field Size in Complex Visual Dysfunctions: A Posterior Cortical Atrophy Model." *JAMA Neurology* 76 (11): 1391–96.

Dijkstra, E. W. 1959. "A Note on Two Problems in Connexion with Graphs." *Numerische Mathematik*. https://doi.org/10.1007/bf01386390.

Dumoulin, Serge O., and Brian A. Wandell. 2008. "Population Receptive Field Estimates in Human Visual Cortex." *NeuroImage* 39 (2): 647–60.

Edwards, David, Gabriel C. G. de Abreu, and Rodrigo Labouriau. 2010. "Selecting High-Dimensional Mixed Graphical Models Using Minimal AIC or BIC Forests." *BMC Bioinformatics*. https://doi.org/10.1186/1471-2105-11-18.

Engel, S. A., G. H. Glover, and B. A. Wandell. 1997.

"Retinotopic Organization in Human Visual Cortex and the Spatial Precision of Functional MRI." *Cerebral Cortex* 7 (2): 181–92.

Gravel, Nicolás, Ben Harvey, Barbara Nordhjem, Koen V. Haak, Serge O. Dumoulin, Remco Renken, Branislava Curčić-Blake, and Frans W. Cornelissen. 2014. "Cortical Connective Field Estimates from Resting State fMRI Activity." *Frontiers in Neuroscience* 8 (October): 339.

Grigorescu, Cosmin, Nicolai Petkov, and Michel A. Westenberg. 2003. "Contour Detection Based on Nonclassical Receptive Field Inhibition." *IEEE Transactions on Image Processing: A Publication of the IEEE Signal Processing Society* 12 (7): 729–39.

Haak, Koen V., Antony B. Morland, Gary S. Rubin, and Frans W. Cornelissen. 2016. "Preserved Retinotopic Brain Connectivity in Macular Degeneration." *Ophthalmic & Physiological Optics: The Journal of the British College of Ophthalmic Opticians* 36 (3): 335–43.

Haak, Koen V., Jonathan Winawer, Ben M. Harvey, Remco Renken, Serge O. Dumoulin, Brian A. Wandell, and Frans W. Cornelissen. 2013. "Connective Field Modeling." *NeuroImage* 66 (February): 376–84.

Haak, K. V., A. B. Morland, and F. W. Cornelissen. 2013. "Connective Field Estimates in the Cortical Lesion Project Zone of Individuals with Macular Degeneration." *Journal of Vision*. https://doi.org/10.1167/13.15.11.

Halbertsma, Hinke N., Koen V. Haak, and Frans W. Cornelissen. 2019. "Stimulus- and Neural-Referred Visual Receptive Field Properties Following Hemispherectomy: A Case Study Revisited." *Neural Plasticity* 2019 (September): 6067871.

Kumano, Hironori, and Takanori Uka. 2010. "The Spatial Profile of Macaque MT Neurons Is Consistent with Gaussian Sampling of Logarithmically Coordinated Visual Representation." *Journal of Neurophysiology* 104 (1): 61–75.

Liu, Jia, Daniel J. Nordman, and William Q. Meeker. 2016. "The Number of MCMC Draws Needed to Compute Bayesian Credible Bounds." *The American Statistician*. https://doi.org/10.1080/00031305.2016.1158738.

Meindertsma, Thomas, Niels A. Kloosterman, Guido Nolte, Andreas K. Engel, and Tobias H. Donner. 2017. "Multiple Transient Signals in Human Visual Cortex Associated with an Elementary Decision." *The Journal of Neuroscience: The Official Journal of the Society for Neuroscience* 37 (23): 5744–57.

Mira, Antonietta. 2008. "Convergence and Mixing in Markov Chain Monte Carlo." *Encyclopedia of Statistics in Quality and Reliability*. https://doi.org/10.1002/9780470061572.eqr478.

Myung, Jay I., and Mark A. Pitt. 2004. "Model Comparison Methods." *Methods in Enzymology*. https://doi.org/10.1016/s0076-6879(04)83014-3.

Papadopoulos, Christos E., and Hoi Yeung. 2001. "Uncertainty Estimation and Monte Carlo Simulation Method." *Flow Measurement and Instrumentation*. https://doi.org/10.1016/s0955-5986(01)00015-2.

Park, Sang-Jae, Jang-Kyoo Shin, and Minho Lee. 2002. "Biologically Inspired Saliency Map Model for Bottom-up Visual Attention." *Biologically Motivated Computer Vision*. https://doi.org/10.1007/3-540-36181-2_42.

Pelli, D. G. 1997. "The VideoToolbox Software for Visual Psychophysics: Transforming Numbers into Movies." *Spatial Vision* 10 (4): 437–42.

Penny, W. D. 2012. "Comparing Dynamic Causal Models Using AIC, BIC and Free Energy." *NeuroImage* 59 (1): 319–30.

Quax, Silvan C., Thomas C. van Koppen, Pasi Jylänki, Serge O. Dumoulin, and Marcel A. J. van Gerven.

n.d. "Slice-Sampled Bayesian PRF Mapping." https://doi.org/10.1101/093724.

Räth, C., and R. Monetti. 2009. "Surrogates with Random Fourier Phases." *Topics on Chaotic Systems*. https://doi.org/10.1142/9789814271349_0031.

Robert, Christian, and George Casella. 2011. "A Short History of Markov Chain Monte Carlo: Subjective Recollections from Incomplete Data." *Statistical Science*. https://doi.org/10.1214/10-sts351.

Robinson, D. A. 1989. "Integrating with Neurons." *Annual Review of Neuroscience* 12: 33–45.

Schreiber, Thomas, and Andreas Schmitz. 1996. "Improved Surrogate Data for Nonlinearity Tests." *Physical Review Letters*. https://doi.org/10.1103/physrevlett.77.635.

Schwarz, Gideon. 1978. "Estimating the Dimension of a Model." *The Annals of Statistics*. https://doi.org/10.1214/aos/1176344136.

Schweitzer, Paul J. 1986. "Posterior Bounds on the Equilibrium Distribution of a Finite Markov Chain." *Communications in Statistics. Stochastic Models*. https://doi.org/10.1080/15326348608807040.

Sereno, Martin I., Colin T. McDonald, and John M. Allman. 1994. "Analysis of Retinotopic Maps in Extrastriate Cortex." *Cerebral Cortex*. https://doi.org/10.1093/cercor/4.6.601.

Thielen, Jordy, Umut Güçlü, Yagmur Güçlütürk, Luca Ambrogioni, Sander E. Bosch, and Marcel A. J. van Gerven. n.d. "DeepRF: Ultrafast Population Receptive Field Mapping with Deep Learning." https://doi.org/10.1101/732990.

Toft, Nils, Giles T. Innocent, George Gettinby, and Stuart W. J. Reid. 2007. "Assessing the Convergence of Markov Chain Monte Carlo Methods: An Example from Evaluation of Diagnostic Tests in Absence of a Gold Standard." *Preventive Veterinary Medicine* 79 (2-4): 244–56.

Wandell, Brian A., and Alex R. Wade. 2003. "Functional Imaging of the Visual Pathways." *Neurologic Clinics* 21 (2): 417–43, vi.

Wandell, Brian A., and Jonathan Winawer. 2015. "Computational Neuroimaging and Population Receptive Fields." *Trends in Cognitive Sciences* 19 (6): 349–57.

Zeidman, Peter, Edward Harry Silson, Dietrich Samuel Schwarzkopf, Chris Ian Baker, and Will Penny. 2018. "Bayesian Population Receptive Field Modelling." *NeuroImage* 180 (Pt A): 173–87.

Zhang, Sheng, Craig K. Abbey, and Miguel P. Eckstein. 2009. "Virtual Evolution for Visual Search in Natural Images Results in Behavioral Receptive Fields with Inhibitory Surrounds." *Visual Neuroscience*. https://doi.org/10.1017/s0952523809090014.

Zuiderbaan, Wietske, Ben M. Harvey, and Serge O. Dumoulin. 2012. "Modeling Center-Surround Configurations in Population Receptive Fields Using fMRI." *Journal of Vision* 12 (3): 10.

SUPPLEMENTARY MATERIAL

S1. MCMC procedure: pseudocode

```
PROGRAM MCMC_Procedure:

Initialise  v0 initial
            lσ initial
            lβ initial
            ls
            w

Starting mcmc loop

      Compute

            ls

              set  ms
                   step
                   v0 proposed

              set  daccepted

              set  dproposed

      Compute CF predictions

      Compute prior and posterior probability of 'accepted' and 'proposed'
variable values

      Compute MLE based on prior and posterior probabilities

      Calculate an acceptance probability ratio

            accept_ratio=p_proposed/p_accepted

          lσ accepted = lσ proposed
          lβ accepted  = lβ proposed
          ls accepted = ls proposed
          daccepted = dproposed

     END

END mcmc loop
```

S2. Difference of Gaussians: bCF$_A$

As for bCF_B described in section 2.5.1, the same MCMC fitting procedure as described in section 2.5 was used. In bCF_A, both σ and σ_2 parameters were retained. For each of the two Gaussian distributions, a predicted weighted fMRI signal $p_1(t)$and $p_2(t)$ was created, respectively. In order to orthonormalize both $p_1(t)$ and $p_2(t)$ signals, the Gram-Schmidt process was applied and the inner product between $p_1(t)$ and $p_2(t)$ was consequently used in the OLS fit. For this DoG bCF model, the initial values of $l_{\sigma 2}$ and $l_{\beta 2}$ were set to 5 and 10, respectively.

S3. Evaluation of beta thresholding

To evaluate the novel thresholding methods in the voxel selection, we consider the (posterior) uncertainty that is related to the residual noise of the model, associated with each bCF parameter, respectively. For each of the threshold techniques, the following thresholds were used: the VE obtained on the null distribution and the effect size that survived the beta thresholds (for more details, see Method 2.6.2). By comparing both the *beta*-uncorrected and *beta*-corrected thresholds (95th percentile) to the VE of the null distribution, we noticed that most voxels with high uncertainty are discarded using the beta-threshold approaches and not the null-based VE (see Figure S2). Therefore, the FWE-corrected *beta* threshold obtained using the 95th percentile is applied in the model comparison analysis.

SUPPLEMENTARY FIGURES

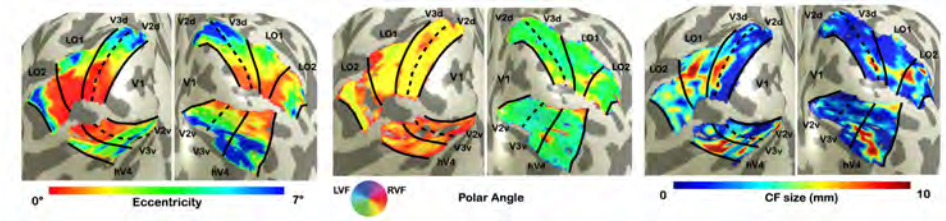

Figure S1. Visualization of bCF_B derived maps for the participant also shown in figure 3. From left to right: eccentricity, polar angle and CF size parameters. Further details as in figure 3.

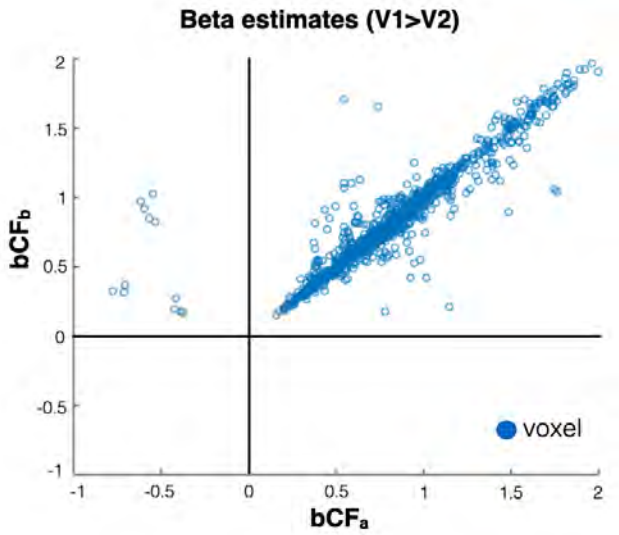

Figure S2 - Voxel-level beta estimates for bCF_A versus bCF_B for a single participant for V1>V2. This example shows that the beta estimates for both options are generally very similar.

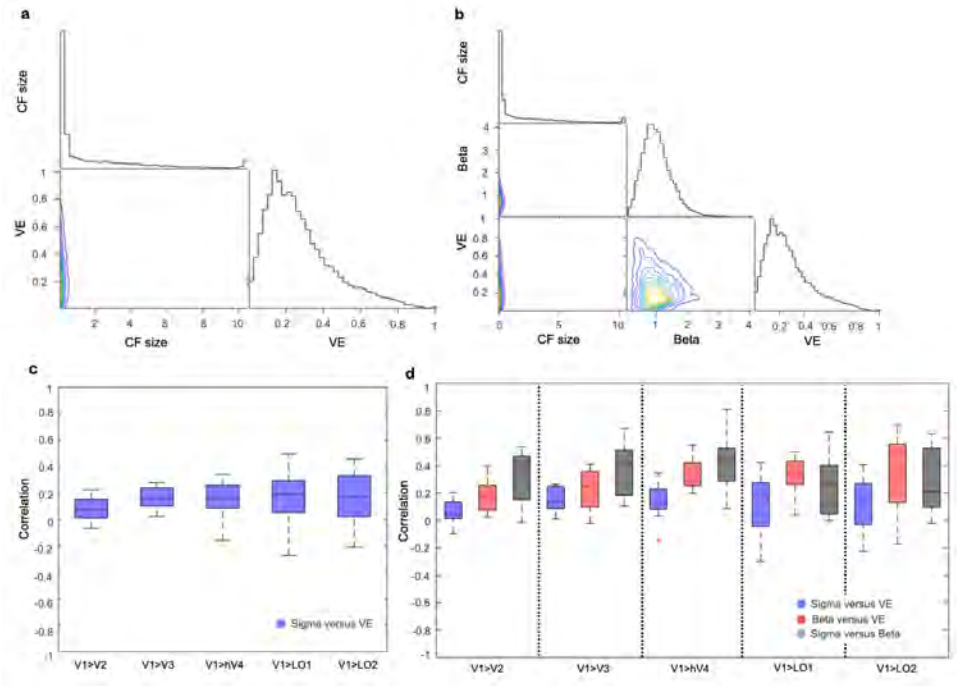

Figure S3 - Dependencies between Bayesian CF parameters at the group level. In panel a and b, the "corner plot" reporting the posterior parameter distribution and off -diagonal, the pairwise distribution between the CF parameters directly estimated using the model (σ, β and VE) is reported for V1>V2. Each correlation was first computed at the participant level and then the median across all participants was computed. In panels c and d, the cross-correlation between the various CF parameters is reported for different ROI. Panels **a** and **c** show the dependencies for bCF_A model while panels **b** and **d** do so for the bCF_B model.

Table S1 - Pearson correlations between the parameter estimates of the standard CF, bCF_A and bCF_B approaches for eccentricity, polar angel, and CF size at the group level per target ROI.

CF versus bCF_a			
ROIs	*Eccentricity*	*Polar Angle*	*CF size*
V1 --> V2	0.719	0.885	0.774
V1 --> V3	0.647	0.745	0.574
V1 -> hV4	0.628	0.746	0.541
V1 -> LO1	0.756	0.551	0.641
V1 -> LO2	0.412	0.646	0.611
CF versus bCF_b			
ROIs	*Eccentricity*	*Polar Angle*	*CF size*
V1 --> V2	0.704	0.829	0.766
V1 --> V3	0.585	0.731	0.611
V1 -> hV4	0.511	0.552	0.528
V1 -> LO1	0.592	0.533	0.501
V1 -> LO2	0.308	0.589	0.585
bCF_a versus bCF_b			
ROIs	*Eccentricity*	*Polar Angle*	*CF size*
V1 --> V2	0.725	0.779	0.747
V1 --> V3	0.655	0.766	0.617
V1 -> hV4	0.71	0.704	0.623
V1 -> LO1	0.666	0.627	0.567
V1 -> LO2	0.549	0.658	0.583

To estimate and compare the level of agreement of CF parameter estimates obtained by using the standard CF and the Bayesian CF models, we correlated the parameter estimates obtained at the participant level and then averaged over the number of participants.

Table S2 - Comparison between pRF, CF and bCF$_A$ parameters at single participant level.

Eccentricity							*Polar Angle*							*CF Size*						
Subject n.1							*Subject n.1*							*Subject n.1*						
	CF		*bCFa*		*bCFa*			*CF*		*bCFa*		*bCFa*			*CF*		*bCFa*		*bCFa*	
ROIs	*Median*	*CI*	*Median*	*CI*	*Median*	*CI*	*ROIs*	*Median*	*CI*	*Median*	*CI*	*Median*	*CI*	*ROIs*	*Median*	*CI*	*Median*	*CI*	*Median*	*CI*
V1 --> V2	2.53	[2.53,2.64]	2.53	[2.53,2.64]	2.71	[2.67,2.75]	*V1 --> V2*	2.51	[2.51,2.57]	2.51	[2.51,2.55]	2.51	[2.51,2.57]	*V1 --> V2*	0.0001	[0.01,0.01]	0.18	[0.18,0.18]	0.21	[0.21,0.22]
V1 --> V3	2.91	[2.86,2.91]	2.91	[2.84,2.91]	2.86	[2.76,2.89]	*V1 --> V3*	2.65	[2.64,2.69]	2.65	[2.64,2.69]	2.71	[2.69,2.74]	*V1 --> V3*	1.43	[1.22,1.43]	1.02	[0.95,1.06]	1.19	[1.13,1.25]
V1 --> hV4	3.64	[3.64,3.71]	3.84	[3.84,3.84]	3.39	[3.39,3.40]	*V1 --> hV4*	3.90	[3.90,3.90]	3.91	[3.90,3.91]	3.95	[3.93,3.96]	*V1 --> hV4*	6.43	[6.33,6.53]	3.33	[3.27,3.39]	4.26	[4.03,4.49]
V1 --> LO1	1.36	[1.36,1.36]	1.36	[1.36,1.36]	1.36	[1.36,1.36]	*V1 --> LO1*	2.47	[2.47,2.47]	2.47	[2.47,2.47]	2.47	[2.47,2.47]	*V1 --> LO1*	5.51	[5.51,5.51]	1.81	[1.58,2.04]	4.67	[4.49,4.89]
V1 --> LO2	3.67	[3.67,3.64]	3.67	[3.67,3.67]	3.67	[3.67,3.67]	*V1 --> LO2*	1.47	[1.47,1.47]	1.47	[1.47,1.47]	1.47	[1.47,1.47]	*V1 --> LO2*	8.16	[8.16,8.16]	7.93	[7.93,7.95]	8.32	[8.29,8.32]
ROIs			*Subject n.2*				*ROIs*			*Subject n.2*				*ROIs*			*Subject n.2*			
V1 --> V2	3.67	[3.64,3.67]	3.66	[3.63,3.67]	3.57	[3.52,3.61]	*V1 --> V2*	1.96	[1.88,2.01]	1.98	[1.88,2.02]	1.98	[1.87,2.01]	*V1 --> V2*	0.61	[0.61,0.61]	0.56	[0.53,0.59]	0.42	[0.38,0.46]
V1 --> V3	3.07	[3.02,3.08]	3.07	[3.02,3.08]	3.06	[2.94,3.07]	*V1 --> V3*	1.37	[1.25,1.46]	1.37	[1.26,1.46]	1.46	[1.36,1.57]	*V1 --> V3*	1.63	[1.63,1.84]	1.64	[1.52,1.71]	1.94	[1.83,2.06]
V1 --> hV4	2.35	[2.35,2.35]	2.35	[2.35,2.35]	2.35	[2.35,2.35]	*V1 --> hV4*	0	[0,0.05]	0	[0,0.05]	0	[0,0]	*V1 --> hV4*	0.41	[0.41,0.41]	0.44	[0.42,0.45]	0.31	[0.29,0.32]
V1 --> LO1	1.49	[1.45,1.53]	1.53	[1.45,1.53]	1.57	[1.58,1.64]	*V1 --> LO1*	1.91	[1.90,1.93]	1.91	[1.91,1.91]	1.91	[1.89,1.91]	*V1 --> LO1*	3.47	[3.18,3.88]	3.97	[3.58,4.07]	4.71	[4.63,4.88]
V1 --> LO2	1.57	[1.46,1.66]	1.57	[1.58,1.59]	1.57	[1.57,1.57]	*V1 --> LO2*	2.51	[2.50,2.50]	2.51	[2.51,2.51]	2.51	[2.47,2.50]	*V1 --> LO2*	4.28	[4.13,4.28]	4.13	[4.07,4.15]	4.34	[4.17,4.38]
ROIs			*Subject n.3*				*ROIs*			*Subject n.3*				*ROIs*			*Subject n.3*			
V1 --> V2	2.89	[2.68,3.02]	2.83	[2.68,3.01]	2.82	[2.68,2.98]	*V1 --> V2*	2.82	[2.75,2.82]	2.82	[2.75,2.88]	2.82	[2.74,2.89]	*V1 --> V2*	0.41	[0.21,0.41]	0.31	[0.25,0.36]	0.34	[0.27,0.33]
V1 --> V3	3.20	[3.16,3.47]	3.20	[3.16,3.47]	3.41	[3.20,3.62]	*V1 --> V3*	3.22	[3.17,3.22]	3.22	[3.17,3.24]	3.22	[3.22,3.25]	*V1 --> V3*	2.86	[2.86,3.06]	2.71	[2.61,2.87]	2.99	[2.87,3.13]
V1 --> hV4	2.21	[2.15,2.25]	2.18	[2.15,2.25]	2.23	[2.15,2.30]	*V1 --> hV4*	3.27	[3.24,3.29]	3.28	[3.25,3.29]	3.28	[3.26,3.29]	*V1 --> hV4*	2.65	[2.25,2.86]	0.89	[0.76,1.19]	1.27	[1.08,1.43]
V1 --> LO1	1.72	[1.72,1.74]	1.72	[1.72,1.72]	1.72	[1.61,1.72]	*V1 --> LO1*	1.88	[1.75,1.88]	1.88	[1.69,1.89]	1.85	[1.26,1.89]	*V1 --> LO1*	0.41	[0.21,0.61]	0.19	[0.18,0.20]	0.33	[0.31,0.37]
V1 --> LO2	2.01	[1.88,2.03]	2.01	[1.93,2.13]	2.04	[1.97,2.16]	*V1 --> LO2*	2.73	[2.65,2.76]	2.73	[2.66,2.73]	2.57	[2.58,2.58]	*V1 --> LO2*	5.41	[4.65,5.72]	1.52	[1.39,1.75]	3.63	[3.39,4.42]
ROIs			*Subject n.4*				*ROIs*			*Subject n.4*				*ROIs*			*Subject n.4*			
V1 --> V2	3.62	[3.30,3.66]	3.76	[3.66,4.07]	3.96	[3.76,4.14]	*V1 --> V2*	3.29	[3.28,3.29]	3.29	[3.29,3.29]	3.29	[3.29,3.35]	*V1 --> V2*	0.01	[0.01,0.01]	0.18	[0.18,0.19]	0.21	[0.18,0.22]
V1 --> V3	2.63	[2.64,2.64]	2.70	[2.64,2.76]	2.79	[2.64,2.93]	*V1 --> V3*	3.29	[3.29,3.29]	3.29	[3.29,3.29]	3.29	[3.29,3.35]	*V1 --> V3*	0.01	[0.01,0.01]	0.21	[0.19,0.24]	0.23	[0.22,0.24]
V1 --> hV4	3.14	[2.85,3.20]	3.20	[2.93,3.21]	3.30	[3.21,3.55]	*V1 --> hV4*	3.64	[3.39,3.64]	3.65	[3.65,3.65]	3.65	[3.65,3.65]	*V1 --> hV4*	0.41	[0.41,0.41]	0.21	[0.20,0.27]	0.26	[0.24,0.27]
V1 --> LO1	2.28	[2.23,2.38]	2.28	[2.22,2.38]	2.23	[2.23,2.25]	*V1 --> LO1*	3.29	[3.23,3.29]	3.28	[3.23,3.29]	3.28	[3.23,3.29]	*V1 --> LO1*	0.01	[0.09,0.21]	0.25	[0.22,0.31]	0.29	[0.27,0.31]
V1 --> LO2	2.62	[2.62,2.62]	2.62	[2.62,2.62]	2.62	[2.62,2.62]	*V1 --> LO2*	3.29	[3.29,3.29]	3.29	[3.29,3.29]	3.29	[3.29,3.29]	*V1 --> LO2*	0.01	[0.01,0.01]	0.18	[0.18,0.18]	0.22	[0.21,0.23]
ROIs			*Subject n.5*				*ROIs*			*Subject n.5*				*ROIs*			*Subject n.5*			
V1 --> V2	4.04	[3.83,4.23]	4.04	[3.83,4.22]	407	[3.83,4.18]	*V1 --> V2*	2.36	[2.27,2.41]	2.36	[2.27,2.41]	2.36	[2.29,2.41]	*V1 --> V2*	1.22	[1.02,1.43]	0.88	[0.72,1.06]	1.13	[0.87,1.45]
V1 --> V3	2.57	[2.57,2.62]	2.57	[2.57,2.60]	2.57	[2.57,2.64]	*V1 --> V3*	2.39	[2.26,2.41]	2.38	[2.25,2.39]	2.36	[2.25,2.39]	*V1 --> V3*	1.02	[0.82,1.23]	0.84	[0.76,1.01]	1.05	[0.86,1.18]
V1 --> hV4	2.57	[2.57,2.62]	2.57	[2.57,2.62]	2.57	[2.57,2.57]	*V1 --> hV4*	2.91	[2.91,2.94]	2.90	[2.91,2.94]	2.91	[2.90,2.94]	*V1 --> hV4*	2.86	[2.48,3.43]	1.42	[1.26,1.86]	2.77	[2.31,3.26]
V1 --> LO1	2.57	[2.49,2.57]	2.57	[2.49,2.57]	2.49	[2.22,2.57]	*V1 --> LO1*	1.05	[0.86,1.05]	0.87	[0.86,1.055]	0.94	[0.86,1.05]	*V1 --> LO1*	2.35	[2.04,2.65]	1.72	[1.59,1.77]	1.84	[1.73,1.97]
V1 --> LO2	4.96	[4.95,4.95]	4.95	[4.95,4.95]	4.95	[4.93,4.95]	*V1 --> LO2*	2.02	[1.97,2.03]	2.03	[1.98,2.05]	1.92	[1.92,1.96]	*V1 --> LO2*	2.24	[2.24,2.34]	2.22	[2.22,2.22]	2.35	[2.31,2.38]
ROIs			*Subject n.6*				*ROIs*			*Subject n.6*				*ROIs*			*Subject n.6*			
V1 --> V2	4.33	[4.18,4.59]	4.18	[4.18,4.55]	4.18	[3.98,4.35]	*V1 --> V2*	3.12	[2.89,3.19]	3.12	[2.89,3.22]	3.12	[2.87,3.17]	*V1 --> V2*	0.82	[0.61,0.82]	0.73	[0.64,0.83]	0.72	[0.58,0.91]
V1 --> V3	2.91	[2.59,3.01]	2.87	[2.61,3.01]	2.80	[2.62,3.00]	*V1 --> V3*	3.17	[3.12,3.22]	3.17	[3.12,3.22]	3.14	[3.12,3.28]	*V1 --> V3*	0.82	[0.82,1.02]	0.94	[0.83,1.05]	1.23	[0.97,1.47]
V1 --> hV4	3.01	[3.01,3.01]	3.01	[3.01,3.01]	3.01	[3.01,3.01]	*V1 --> hV4*	3.85	[3.84,3.85]	3.85	[3.85,3.85]	3.77	[3.73,3.79]	*V1 --> hV4*	0.41	[0.41,0.41]	0.45	[0.43,0.47]	0.36	[0.29,0.38]
V1 --> LO1	1.26	[1.25,1.26]	1.25	[1.25,1.26]	1.26	[1.25,1.67]	*V1 --> LO1*	2.86	[2.81,2.87]	2.87	[2.83,2.87]	2.87	[2.83,2.87]	*V1 --> LO1*	2.24	[1.84,2.45]	2.14	[1.83,2.38]	2.15	[1.80,2.47]
V1 --> LO2	1.17	[0.94,1.48]	0.94	[0.94,1.48]	0.94	[0.94,1.11]	*V1 --> LO2*	3.17	[3.17,3.22]	3.17	[3.17,3.17]	3.17	[3.17,3.17]	*V1 --> LO2*	1.43	[1.43,1.63]	1.57	[1.49,1.69]	1.32	[1.18,1.41]
ROIs			*Subject n.7*				*ROIs*			*Subject n.7*				*ROIs*			*Subject n.7*			
V1 --> V2	3.11	[2.75,3.38]	3.25	[2.77,3.35]	3.09	[2.75,3.29]	*V1 --> V2*	3.66	[3.56,3.69]	3.66	[3.56,3.69]	3.66	[3.58,3.69]	*V1 --> V2*	2.86	[2.65,3.26]	2.68	[2.50,2.83]	2.84	[2.53,2.98]
V1 --> V3	2.82	[2.72,3.23]	2.79	[2.66,3.12]	2.77	[2.48,3.09]	*V1 --> V3*	3.56	[3.42,3.66]	3.48	[3.42,3.66]	3.56	[3.46,3.66]	*V1 --> V3*	3.87	[3.67,4.08]	3.47	[3.29,3.64]	3.51	[3.35,3.72]
V1 --> hV4	1.34	[1.29,1.46]	1.34	[1.29,1.42]	1.34	[1.25,1.47]	*V1 --> hV4*	4.71	[4.46,5.18]	4.71	[4.46,5.17]	4.71	[4.71,5.23]	*V1 --> hV4*	4.28	[3.87,4.69]	3.57	[2.77,4.04]	3.59	[3.21,3.92]
V1 --> LO1	3.56	[3.56,3.56]	3.56	[3.56,3.56]	3.56	[3.33,3.56]	*V1 --> LO1*	1.27	[1.27,1.32]	1.27	[1.27,1.30]	1.27	[1.27,1.33]	*V1 --> LO1*	3.47	[3.26,3.67]	3.34	[3.21,3.48]	3.45	[3.36,3.64]
V1 --> LO2	3.56	[3.56,3.56]	3.56	[3.56,3.56]	3.56	[3.27,3.56]	*V1 --> LO2*	1.32	[1.27,2.13]	1.27	[1.25,1.32]	1.33	[1.27,2.38]	*V1 --> LO2*	4.49	[4.33,4.48]	4.41	[4.29,4.49]	4.98	[4.87,5.07]
ROIs			*Subject n.8*				*ROIs*			*Subject n.8*				*ROIs*			*Subject n.8*			
V1 --> V2	2.74	[2.45,2.84]	2.70	[2.45,2.81]	2.55	[2.32,2.81]	*V1 --> V2*	1.43	[1.23,1.96]	1.36	[1.23,1.93]	1.37	[1.23,2.03]	*V1 --> V2*	2.25	[1.63,2.65]	1.80	[1.24,2.33]	2.24	[1.53,2.79]
V1 --> V3	2.84	[2.60,2.91]	2.84	[2.49,2.91]	2.84	[2.49,2.91]	*V1 --> V3*	2.15	[2.07,2.34]	2.15	[2.03,2.18]	2.15	[2.09,2.34]	*V1 --> V3*	2.86	[2.65,3.26]	2.77	[2.50,3.06]	2.97	[2.61,3.35]
V1 --> hV4	2.05	[2.05,2.05]	2.05	[2.05,2.05]	2.05	[2.05,2.08]	*V1 --> hV4*	3.55	[3.55,3.61]	3.56	[3.55,3.61]	3.61	[3.56,3.60]	*V1 --> hV4*	3.06	[3.06,3.26]	2.99	[2.92,3.15]	3.06	[2.92,3.32]
V1 --> LO1	0.94	[0.81,1.25]	0.81	[0.76,1.24]	0.81	[0.76,0.94]	*V1 --> LO1*	1.05	[1.05,1.23]	1.05	[1.05,1.23]	1.05	[1.05,1.15]	*V1 --> LO1*	5.92	[5.72,6.33]	5.26	[4.96,5.65]	5.33	[5.11,5.66]
V1 --> LO2	0.94	[0.82,1.05]	0.81	[0.78,0.94]	0.80	[0.62,0.94]	*V1 --> LO2*	1.43	[1.05,2.38]	1.43	[1.05,2.09]	1.38	[1.05,2.28]	*V1 --> LO2*	7.45	[6.73,8.57]	6.38	[6.05,6.51]	6.06	[6.03,6.28]
ROIs			*Subject n.9*				*ROIs*			*Subject n.9*				*ROIs*			*Subject n.9*			
V1 --> V2	3.33	[3.21,3.46]	3.39	[3.21,3.46]	3.34	[3.06,3.46]	*V1 --> V2*	3.45	[3.34,3.55]	3.45	[3.38,3.55]	3.44	[3.34,3.55]	*V1 --> V2*	0.41	[0.41,0.61]	0.46	[0.34,0.61]	0.37	[0.32,0.54]
V1 --> V3	3.21	[2.96,3.46]	3.18	[2.89,3.46]	3.21	[2.96,3.46]	*V1 --> V3*	3.15	[2.91,3.35]	3.09	[2.88,3.33]	3.06	[2.70,3.31]	*V1 --> V3*	2.45	[2.04,2.65]	2.06	[1.76,2.27]	2.20	[1.96,2.49]
V1 --> hV4	3.27	[2.98,3.46]	3.21	[2.78,3.46]	3.13	[2.97,3.45]	*V1 --> hV4*	4.53	[3.77,5.10]	4.97	[3.81,5.10]	4.18	[3.74,5.01]	*V1 --> hV4*	2.45	[2.04,2.65]	2.05	[1.88,2.32]	2.45	[2.11,2.96]
V1 --> LO1	1.88	[1.86,1.94]	1.88	[1.86,1.88]	1.88	[1.81,2.28]	*V1 --> LO1*	3.17	[3.14,3.25]	3.17	[3.14,3.25]	3.14	[3.09,3.26]	*V1 --> LO1*	2.86	[2.65,2.93]	2.74	[2.65,2.86]	3.21	[2.87,3.62]
V1 --> LO2	1.64	[1.54,1.69]	1.59	[1.42,1.63]	1.62	[1.40,1.63]	*V1 --> LO2*	1.17	[1.12,1.38]	1.12	[1.11,1.36]	1.29	[1.14,1.42]	*V1 --> LO2*	2.65	[2.04,3.06]	1.41	[1.17,1.67]	2.63	[1.97,2.72]
ROIs			*Subject n.10*				*ROIs*			*Subject n.10*				*ROIs*			*Subject n.10*			
V1 --> V2	3.73	[3.07,4.03]	3.74	[3.09,4.03]	3.74	[3.19,4.03]	*V1 --> V2*	2.84	[2.65,3.34]	2.77	[2.64,3.32]	2.84	[2.65,3.34]	*V1 --> V2*	1.02	[0.61,1.23]	0.84	[0.55,1.15]	0.69	[0.44,0.97]
V1 --> V3	2.61	[2.29,2.85]	2.49	[2.29,2.81]	2.29	[2.20,2.63]	*V1 --> V3*	2.67	[1.59,3.66]	3.14	[1.79,3.74]	3.43	[2.66,3.81]	*V1 --> V3*	1.63	[1.43,2.04]	1.65	[1.42,2.04]	1.95	[1.52,2.27]
V1 --> hV4	2.41	[2.19,2.86]	2.41	[2.19,2.86]	2.40	[2.22,2.66]	*V1 --> hV4*	4.18	[4.01,4.18]	4.18	[4.01,4.18]	4.11	[3.97,4.18]	*V1 --> hV4*	3.06	[2.28,3.67]	2.28	[2.03,2.94]	2.77	[2.23,3.15]
V1 --> LO1	0.83	[0.81,1.21]	0.83	[0.82,1.13]	0.83	[0.82,1.20]	*V1 --> LO1*	1.09	[1.05,1.35]	1.06	[1.05,1.35]	1.05	[1.02,1.11]	*V1 --> LO1*	1.84	[1.63,2.04]	1.86	[1.58,2.03]	1.65	[1.56,1.95]
V1 --> LO2	2.06	[1.92,2.20]	1.92	[1.92,2.20]	2.20	[2.20,2.30]	*V1 --> LO2*	1.97	[1.85,2.21]	1.62	[1.03,1.90]	1.67	[1.05,1.84]	*V1 --> LO2*	0.82	[0.612,0.83]	0.88	[0.84,1.01]	2.07	[1.82,2.47]
ROIs			*Subject n.11*				*ROIs*			*Subject n.11*				*ROIs*			*Subject n.11*			
V1 --> V2	3.96	[3.52,4.51]	3.96	[3.52,4.51]	3.85	[3.51,4.52]	*V1 --> V2*	3.77	[3.66,3.89]	3.77	[3.665,3.89]	3.75	[3.66,3.88]	*V1 --> V2*	2.04	[1.84,2.25]	1.94	[1.71,2.25]	2.01	[1.71,2.27]
V1 --> V3	3.17	[2.92,3.38]	3.17	[2.92,3.28]	3.08	[2.87,3.17]	*V1 --> V3*	2.72	[2.21,3.55]	2.73	[2.21,3.55]	2.73	[2.18,3.55]	*V1 --> V3*	3.26	[2.65,4.28]	3.25	[2.64,4.22]	3.47	[2.77,4.21]
V1 --> hV4	3.28	[3.08,3.52]	3.28	[3.08,3.52]	3.51	[3.18,4.01]	*V1 --> hV4*	3.77	[3.74,3.86]	3.74	[3.74,3.83]	3.82	[3.75,3.87]	*V1 --> hV4*	2.45	[2.04,3.06]	1.96	[1.59,2.45]	2.20	[1.79,2.65]
V1 --> LO1	1.22	[1.22,1.22]	1.22	[1.22,1.22]	1.22	[1.22,1.22]	*V1 --> LO1*	1.34	[1.25,1.68]	1.34	[1.25,1.65]	1.31	[1.25,1.66]	*V1 --> LO1*	3.87	[3.26,4.69]	3.63	[3.27,4.18]	4.07	[3.65,4.60]
V1 --> LO2	1.69	[1.37,1.83]	1.25	[1.25,1.63]	0.84	[0.84,0.86]	*V1 --> LO2*	3.47	[3.41,3.47]	3.47	[3.47,3.86]	3.32	[3.28,3.34]	*V1 --> LO2*	2.24	[2.09,2.68]	2.12	[2.05,2.18]	2.52	[2.12,2.93]
ROIs			*Subject n.12*				*ROIs*			*Subject n.12*				*ROIs*			*Subject n.12*			
V1 --> V2	3.39	[2.96,3.59]	3.39	[2.96,3.62]	3.39	[2.98,3.75]	*V1 --> V2*	1.05	[0.97,2.43]	1.05	[0.97,2.44]	1.03	[0.97,2.43]	*V1 --> V2*	3.47	[3.06,3.87]	3.39	[2.89,3.73]	3.48	[3.01,3.99]
V1 --> V3	3.14	[2.82,3.52]	3.14	[2.79,3.39]	3.14	[2.85,3.54]	*V1 --> V3*	2.43	[2.09,3.14]	2.45	[2.10,3.15]	2.62	[2.10,3.19]	*V1 --> V3*	4.49	[3.47,5.31]	4.43	[3.36,5.18]	4.47	[3.65,5.17]
V1 --> hV4	1.63	[1.53,1.63]	1.63	[1.53,1.64]	1.63	[1.53,2.05]	*V1 --> hV4*	3.76	[3.57,3.92]	3.79	[3.66,3.92]	3.74	[3.66,3.91]	*V1 --> hV4*	6.12	[5.31,6.94]	4.94	[4.52,5.19]	5.36	[4.71,5.81]
V1 --> LO1	1.77	[1.63,1.88]	1.69	[1.62,1.88]	1.77	[1.63,1.88]	*V1 --> LO1*	2.43	[2.10,2.43]	2.43	[2.10,2.43]	2.43	[2.10,2.43]	*V1 --> LO1*	5.51	[4.20,6.73]	1.16	[1.02,3.45]	3.94	[1.44,5.37]
V1 --> LO2	1.77	[1.77,1.88]	1.77	[1.65,1.88]	1.81	[1.65,1.88]	*V1 --> LO2*	2.58	[2.43,2.92]	2.61	[2.43,2.89]	2.85	[2.61,2.98]	*V1 --> LO2*	8.77	[8.39,9.39]	1.42	[1.03,6.25]	4.89	[1.15,7.18]

To estimate and compare the level of agreement of CF maps, we computed the correlations between eccentricity (*rho*) and polar angle (*theta*) parameters obtained using the standard CF and Bayesian CF models to the pRF *rho* and *theta (*gold standard).